Dr. Jordi Bonet Ruiz
Chemical Engineering Department

Dr. Joan Llorens Llacuna
Chemical Engineering Department

Grau en Enginyeria Química

Treball Final de Grau

CFD model of an experimental unit for CO_2 adsorption from exhaust gases

Model CFD d'una unitat experimental d'adsorció de CO_2 a partir de gasos d'escapament

Erika Fernández Pizarro

June 2020

UNIVERSITAT DE BARCELONA

Res en la vida ha de ser temut, només comprés.

Ara és el moment de comprendre més, per témer menys.

Marie Curie

Primerament, agrair als meus tutors pel seu recolzament en aquests temps difícils fent possible la continuació del treball via online, guiant-me durant el projecte amb els recursos disponibles, i sobretot per saber-me aconsellar sobre quin enfocament donar-li al treball. A la meva parella i família per donar-me suport i animar-me quan pensava que no podria amb tot i necessitava algú que estigués al meu costat, i per últim, als meus companys de classe, ja que durant el nostre viatge junts hem crescut com a persones i ens emportem grans experiències que ens acompanyaran tota la vida.

CONTENTS

SUMMARY

Carbon dioxide (CO_2) is the largest anthropogenic greenhouse gas (GHG) on the planet contributing to the global warming. Currently, there are three capture technologies of trapping CO_2 from the flue gases: pre-combustion, post-combustion and oxy-fuel combustion. Among these, the post-combustion is widely popular as it can be retrofitted for a short to medium term without encountering any significant technology risks or changes.

Zeolites, also known as molecular sieves, are widely used as a universal separation medium with series of advantages compared to the first-generation capture processes based on amine-based scrubbing.

The goal of this study is to model a reversible adsorption column that prevents the emission of CO_2 from exhaust gases into the atmosphere using the Faujasite 13X as an adsorbent. In addition, the dependence of the particle diameter, the column diameter and the temperature with the breaking time has been studied.

The mathematical model described by *Chatzopoulos & Varma (1995)* has been followed, using the Langmuir isotherm to relate the concentration between solid and gas phase.

The data used is from the vehicle Peugeot 307 gasoline model to calculate the difference in CO_2 emissions with and without the adsorption columns. In addition, a graphic representation of the CO_2 concentration within the column has been made in both phases and a 3D sketch of the boot with the columns incorporated.

Keywords: CO_2 capture, zeolites, weather emergency, global warming.

RESUM

El diòxid de carboni (CO_2) és el major gas d'efecte hivernacle d'origen antropogènic (GEH) del planeta que contribueix a l'escalfament global. Actualment, hi ha tres tecnologies de captura de CO_2 dels gasos de combustió: la combustió prèvia, la post-combustió i l'oxicombustió. Entre aquests, la post-combustió és àmpliament popular, ja que es pot reajustar a curt o mig termini sense presentar riscos ni canvis tecnològics importants.

Les zeolites, també conegudes com tamisos moleculars, s'utilitzen àmpliament com a mitjà de separació universal amb una sèrie d'avantatges en comparació amb els processos de captura de primera generació basats en la depuració a base d'amines.

L'objectiu d'aquest estudi és modelar una columna d'adsorció reversible que eviti l'emissió de CO_2 dels gasos d'escapament a l'atmosfera utilitzant la Faujasita 13X com a adsorbent. A més, s'ha estudiat la dependència del diàmetre de partícula, el diàmetre de la columna i la temperatura amb el temps de ruptura.

S'ha seguit el model matemàtic descrit per *Chatzopoulos i Varma (1995),* utilitzant la isoterma de Langmuir per relacionar la concentració entre la fase sòlida i la fase gas.

Les dades utilitzades provenen del model de benzina Peugeot 307 per calcular la diferència d'emissions de CO_2 amb i sense les columnes d'adsorció. A més, s'ha realitzat una representació gràfica de la concentració de CO_2 dins de la columna en ambdues fases i un croquis 3D del maleter amb les columnes incorporades.

Paraules clau: Captura de CO_2, zeolites, emergència climàtica, escalfament global.

1. INTRODUCTION

In this chapter, we will see what the greenhouse effect is and how human activity, especially transport, has increased the amount emitted of CO_2, one of the main greenhouse gases. We will present the current European regulations in order to reduce these emissions, and different methods to capture CO_2. Among these, we will focus on adsorption, using Faujasite 13X as an adsorbent.

The Earth is constantly bombarded with enormous amounts of radiation, primarily from the sun, which strikes the planet's atmosphere in the form of visible light, plus ultraviolet (UV), infrared (IR) and other types of radiation that are invisible to the human eye.

About 30% of the radiation striking Earth's atmosphere is immediately reflected out to space by clouds, ice, snow, sand and other reflective surfaces, but the remaining 70% of incoming solar radiation is absorbed by the oceans, the land and the atmosphere according to *Mann (2019)*. As they heat up, the oceans, land and atmosphere release heat in the form of thermal radiation, which passes out of the atmosphere and into space. It is this equilibrium of incoming and outgoing radiation that makes the Earth habitable, and it is often referred to as the greenhouse effect because a greenhouse works in much the same way.

However, human activities are changing Earth's natural greenhouse effect by increasing the greenhouse gases, for example burning fossil fuels like coal and oil produce CO_2, which will be studied in detail in the next section.

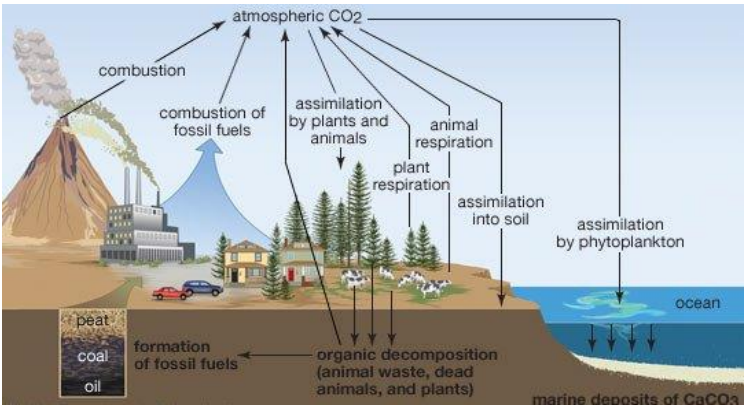

Figure 1. Greenhouse process *(Mann, 2019)*

1.1. GREENHOUSE GASES

Greenhouse gases are gas molecules that absorb thermal infrared radiation, and in enough quantity, can produce the gradual heating of Earth's atmosphere and surface: the global warming.

Since the dawn of the Industrial Revolution in the early 1800s, the burning of fossil fuels like coal, oil and gasoline have greatly increased the concentration of greenhouse gases in the atmosphere, especially CO_2.

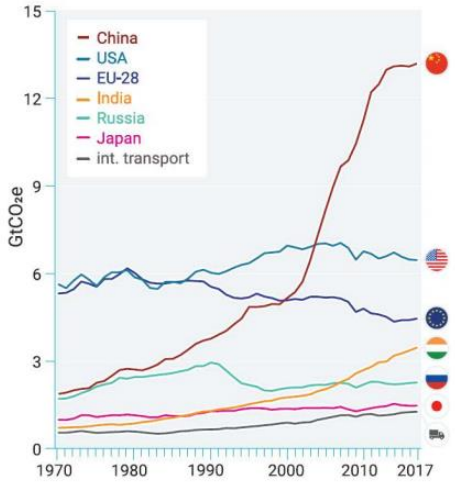

Figure 2. Greenhouse gases emissions for major global economies. *(United Nations, 2018)*

1.1.1. Carbon Dioxide

According to the *United States Environmental Protection Agency (EPA)*, the atmospheric CO_2 levels have increased by more than 40% since the beginning of the Industrial Revolution, from about 280 parts per million (ppm) in the 1800s to more than 400 ppm today. The main human activity that emits CO_2 is the combustion of fossil fuels (coal, natural gas, and oil) for energy and transportation. In 2017, CO_2 accounted for about 81,6% of all U.S. greenhouse gas emissions from human activities:

Transportation: The combustion of fossil fuels such as gasoline and diesel to transport people and goods, including transportation sources such as highway vehicles, air travel, marine transportation, and rail.

Electricity: It is a significant source of energy and is used to power homes, business, and industry. The type of fossil fuel used to generate electricity will emit different amounts of CO_2.

Industry**:** Many industrial processes emit CO_2 through fossil fuel consumption. Several processes also produce CO_2 emissions through chemical reactions that do not involve combustion; for example, the production and consumption of mineral products such as cement, the production of metals such as iron and steel, and the production of chemicals.

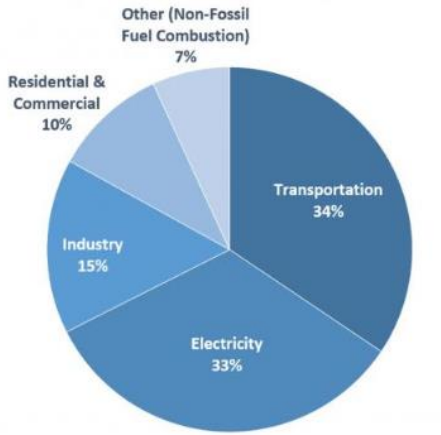

Figure 3. U.S. Carbon Dioxide Emissions by sectors.

(*United States Environmental Protection Agency (EPA)).*

Figure 3 shows that transport has an important contribution to global CO_2 emissions, for this reason in the next section we will focus on vehicle emissions.

1.2. VEHICLE EXHAUST GASES AND POLLUTANTS

According to *Sassykova et al (2019),* cars emit a potent cocktail of exhaust gases, including non-toxic gases like N_2, H_2O, O_2, some noble gases, and toxic gases like:

Carbon dioxide (CO_2): Major contributing factor to climate change, although technically non-toxic, excessive volumes contribute towards ocean acidification.

Carbon monoxide (CO): This invisible gas is the result of incomplete combustion of fuel and is very toxic to humans. Fortunately, most modern engines only produce tiny amounts of it thanks to efficient combustion processes.

Nitrogen oxides (NO_x): Nitrogen oxides are produced in any combustion process; they are highly reactive and can contribute to smog when they contact other airborne chemicals.

Sulphur dioxide (SO_2): This is a colourless gas that smells like burnt matches and occurs naturally in crude oil used to refine petrol and diesel. It forms acids when burned, leading to engine corrosion and smog.

Hydrocarbons (HC): HCs escape from exhausts as unburnt fuel due to incomplete combustion, they also evaporate from the fuel tank and nozzle when you fill up at the petrol station.

Particulates: Diesel engines emit airborne particles of black soot and metal, known as particulate matter. Modern cars are fitted with diesel particulate filters (DPFs) to stop these harmful particles being pumped out into the atmosphere.

The exact composition of exhaust gases depends on the type of engine, but here is an approximation.

Table 1. Composition of exhaust gases of gasoline engines. (*Sassykova et al (2019)*)

Components	Gasoline engine (%Vol.)
Nitrogen	74 - 79
Oxygen	0.3 - 8
Water	13 - 15
Carbon dioxide	5 - 14
CO	1 - 10
NOx	0.1 - 0.5
SOx	0 - 0.002
Hydrocarbons	0.01 - 0.1

Looking at the table above, we can see that by far the greatest portion of the exhaust gases is represented by nitrogen, but in the second place is CO_2. The transition into electric vehicles is being committed, but they remain economically more expensive and with certain barriers in terms of autonomy, so in the meantime, measures must be applied to reduce the CO_2 emitted by conventional cars.

1.3. EUROPEAN LEGISLATION APPLIED IN SPAIN

According to the *Gobierno de España (2014)*, each member state of the UE must limit or reduce its diffuse emissions as established in the Annex II of the Effort Sharing Decision. In the case of Spain, that objective is a reduction in the year 2020 of 10% compared to the levels of 2005.

The European Commission has worked with member states in determining annual allocations emissions (AEAs) in terms of units of carbon dioxide equivalent (CO_2eq) and annual limits of issue for each member state. This work is translated into the following two decisions:

2013/162 / EU: Commission decision on March 26, 2013 by that the annual emission allocations of the member States are determined for the period from 2013 to 2020, in accordance with decision No. 406/2009 / EC of the European Parliament and of the Council.

2013/634 / EU: Commission implementing decision on 31 October 2013 on the adjustments of the annual allocations of emissions of member states for the period 2013-2020 in accordance with the decision 406/2009 / EC of the European Parliament and of the Council.

Table 2. Annual emission allocations for Spain.

Year	2013	2014	2015	2016	2017	2018	2019	2020
AEAs($ktCO_2eq$)	220903	219144	217384	215625	213866	212107	210347	208588

Each member state has the obligation to prepare and present biennially the projections of greenhouse gas emissions of its country. This obligation was regulated by Decision 280/2004/EC, which was recently replaced by Regulation 525/2013/EC.

Table 3. Projections of GHG for Spain between 2013-2020.

Year	2013	2014	2015	2016	2017	2018	2019	2020
kt CO_2 eq	216445	217096	218428	219911	221859	224086	226195	228455

From the analysis of the information contained in the tables above, it can be seen during the first two years of the compliance period, the expected trend of emissions is less than the compliance path, because there is a surplus in allocations.

However, from the third year (2015), the expected emissions exceed the emission allocations for 54.5 $MtCO_2eq$. The expected evolution in terms of deficit and surplus of annual emission allocations must be analysed in the context of Article 3.3 of Decision 406/2009/EC. This establishes that a member state may carry over to the following years the part of its annual emission allocation for a given year, which exceeds its greenhouse gas emissions in that year. In this way, the possibility of establishing an alternative path that takes into account the latter is considered.

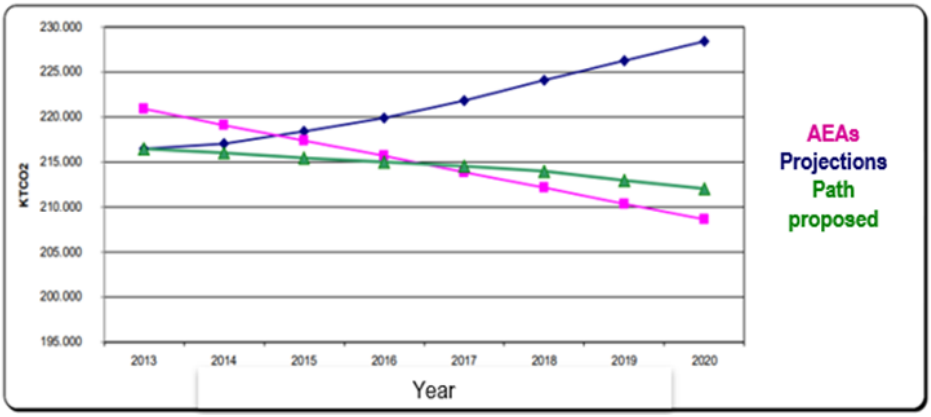

Figure 4. Path proposed.

Total transport emissions in 2011 were 83.6 million tCO_2eq, of which 95% were emissions associated with road transport, with the contribution from the rest of the modes being very minor. Regarding the total national emissions, transport represents 24% of the total and approximately 40% of the emissions from the diffuse sectors, for this reason different CO_2 capture methods will be presented.

1.4. CO2 CAPTURE METHODS

1.4.1. Absorption

Chemical absorption of CO_2 from flue gases using aqueous solvents, mainly alkanolamines like ethanolamine (MEA) is a well-known process, studied in detail. Modern research aims to optimize this process, maximizing the absorption rates and minimizing energy requirements for solvent regeneration.

As part of the natural gas value chain, the well stream must be processed and conditioned. In this process, impurities such as CO_2 and H_2S are removed down to a level that satisfies specifications for LNG production or pipeline transport. Moreover, the water content must be reduced in order to avoid liquefaction and hydrates in the gas pipelines. Flue gases from fossil fuel combustion contains CO_2 that should be removed for greenhouse gas control, and SO_2 (sulphur dioxide), that must be controlled to very low levels. For these applications, chemical absorption is the most common purification technology and the most common method used by industrial large-scale plants for of solving challenges related to gas separation according to *Luis (2015)*.

However, the operation fluctuations and disturbances, such as load variations or start-up mode must be reflected in the process, justifying the emerging need for dynamic modelling. Dynamic analysis is not always realizable as dynamic experimental data are scarce to enable accurate model validation. We cannot carry an absorption and rectification column to car equipment ports and therefore cannot be applied to transportation.

1.4.2. Adsorption

The adsorption is based on the difference of the interaction forces between the flow gases and the surface of a solid, called adsorbent. If one specie is adsorbed more than the others, it starts to accumulate in the adsorbent and disappears from the gas flow, obtaining a purified gas.

By the breakthrough curves, many parameters can be determined as total time to saturate the full column, the breaking point and the mass transfer zone according to *Chowdhury et al (2015)*.

Breaking point: Point at which the concentration of the gas leaving the bed is equal to a maximum concentration value stablished (maximum amount of adsorbate that can be acceptably lost). This study reaches the breaking point when the CO_2 concentration at the outlet is 0,05 (5% of the CO_2 at the inlet). When the breaking point is reached, the flow through this column is stopped and it is redirected to another of the six adsorption columns installed.

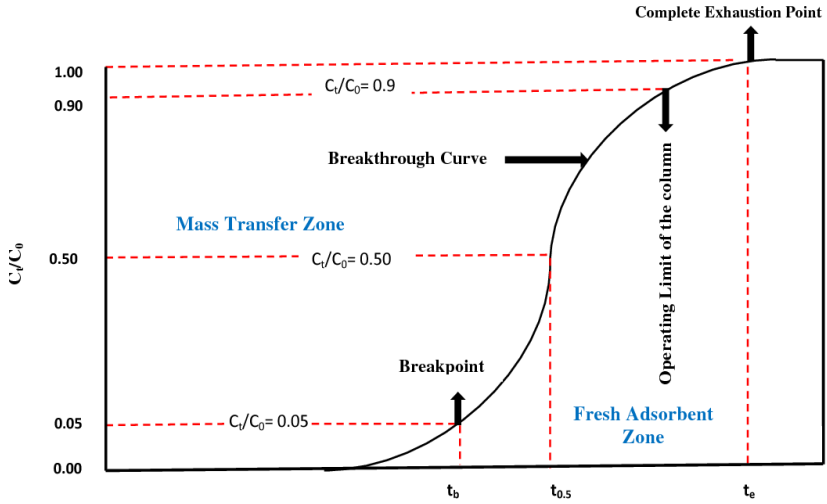

Figure 5. Breaking point example. *(Chowdhury et al, 2015)*

Mass transfer zone: As the concentration wave moves through the bed, most of the mass transfer occurs in a small region. This mass transfer zone moves through the bed until it "breaks through". The shape of the mass transfer zone depends on the adsorption isotherm (equilibrium expression), flow rate, and diffusion characteristics.

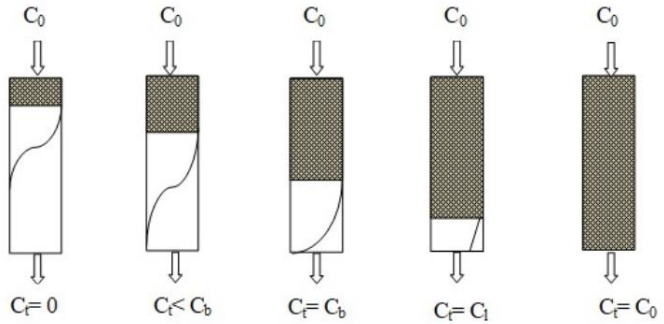

Figure 6. Mass transfer zone example. *(Chowdhury et al, 2015)*

Reversible vs irreversible adsorption

Table 4. Differences between physical and chemical adsorption.

PHYSICAL ADSORPTION	CHEMICAL ADSORPTION
Van der Waals forces	Chemical links
Exothermic character (1-10 kcal/mol)	Exothermic character (10-100 kcal/mol)
Fast kinetics	Slow kinetics
Reversible	Irreversible
On all solids and on its entire surface	At certain solids and at certain points
Low selectivity	High selectivity

The temperature range for reversible adsorption is 25-60ºC according to *Hauchhum & Mahanta (2014)*, therefore an average value of 40ºC has been chosen as the constant operating temperature during the process.

1.5. ADSORBENT SELECTION

It is important to choose a suitable adsorbent for the desired process, for this reason several factors must be considered when choosing. The most important attributes of an adsorbent for any application are capacity, selectivity, regenerability, kinetics, compatibility and surface area according to *Matz & Knaebel (1990)*.

Capacity: Also known as loading, is the amount of adsorbate taken up by the adsorbent, per unit mass (or volume) of the adsorbent. Typically, adsorption capacity data are gathered at a fixed temperature and various adsorbate concentrations, and the data are plotted as an isotherm (loading vs concentration at constant temperature).

Selectivity: Is the ratio of the capacity of one component to that of another at a given fluid concentration.

Regenerability: All cyclic adsorption applications rely on regenerability, so that the adsorbent can operate in sequential cycles with uniform performance. This means each adsorbable component must be relatively weak adsorbed.

Kinetics: Mass transfer kinetics is a catch-all term related to intraparticle mass transfer resistance. It is important because it controls the cycle time of a fixed bed adsorption process. Fast kinetics provide a sharp breakthrough curve, while slow kinetics yields a distended breakthrough curve.

Compatibility: It covers various possible modes of chemical and physical attack that could reduce the life expectancy of the adsorbent.

Surface area: It is the amount of material a sorbent has available for contact and determines the capacity of material a sorbent can capture, the capture rate of the sorbent, and the retention rate of the substance within the sorbent.

1.5.1. Zeolites (Faujasite 13X)

Most zeolites are aluminosilicates which could be thought of as stoichiometric blends of the two previous adsorbents, silica and alumina. They are generally white, opaque and chalk-like in appearance. Zeolites that have significant alumina content are hydrophilic and basic, while those that are predominately silica are hydrophobic and acid. Internally, zeolites are inherently crystalline and exhibit micropores within those crystals that have uniform dimensions. The micropores are so small and uniform that they commonly can distinguish nearly identically sized molecules.

Frequently, there is water from hydration within the crystals, and in order to balance the charges cations are associated with the alumina. The common empirical formula for a zeolite containing a single cation(M), of valence(n) is:

$$\boldsymbol{M_{2/n} * Al_2O_3 * X_{sit} * y\, H_2O}$$ (*Matz & Knaebel, 1990)*

Where X is the silica-to-alumina ratio (generally between 1 to 5) and y is the molar water of hydration. Applications of zeolites include gas or liquid drying, separation of oxygen from the air, or in Pressure Swing Adsorption (PSA) and Temperature Swing Adsorption (TSA) processes to capture CO_2.

Table 5. Commercial Zeolites Characteristics. (*Matz & Knaebel, 1990)*

Zeolite type	Cationic Form	Si/Al ratio
3A	K	1
4A	Na	1
5A	Ca	1
10X	Ca	1.2
13X	**Na**	**1.2**
Y	K	2.4
Mordenite	Na	5

The Faujasite 13X dehydrated composition is $\mathbf{Na_{88}\ Al_{88}\ Si_{104}\ O_{384}}$ according to *Baerlocher et al (1995)* and its basic building blocks are silica and alumina tetrahedron (pyramids). Each tetrahedron consists of a silicon or aluminium atom at the centre of the tetrahedron, with oxygen atoms at the four corners.

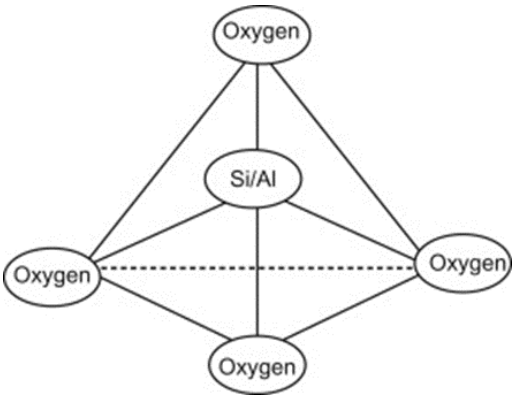

Figure 7. Silica and alumina pyramids. *(Chemical Structure)*

Silicon is in +4 oxidation state, therefore a tetrahedron containing silicon is in neutral charge, in contrast a tetrahedron containing aluminium in oxidation state +3 has a net charge of -1, which must be balanced by a positive ion.

In the case of the Faujasite 13X this positive ion is sodium (Na), with the Si / Al ratio is between 1 and 1.4, that means the higher the ratio, the lower the number of cations needed since there is more silicon that forms neutral tetrahedron.

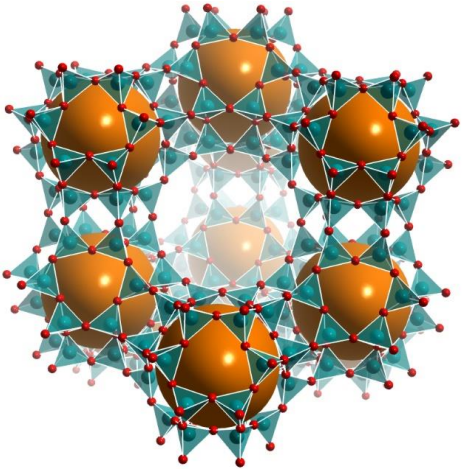

Figure 8. Faujasite 13X 3D structure. *(Chemical Structure)*

As can be seen in figure 15, Faujasite 13X has a Si/Al ratio bigger than 1, which means that it contains more silicate than alumina, hence tends to have hydrophobic behaviour. This benefits us since in the combustion gases emitted by cars approximately 15% is water vapor, and we are not interested in our adsorbent capturing it. Furthermore, due to its crystalline structure, it has micropores that are so small and uniform that they provide very high capacity, selectivity with CO_2, and high surface area, exactly what we need.

Therefore, as a result of what we have stated, it is necessary to avoid the emission of CO_2 into the atmosphere, in this case by adsorption with Faujasite 13X, which is what the present work focuses on.

2. OBJECTIVES

The column has been studied using CFD (Computational Fluid Dynamics) implementing the *Chatzopoulos & Varma (1995)* model in Mathematica software. With the implemented program, it is possible to obtain data at different values of revolutions and displacements of different vehicles. Specifically, we have focused on the Peugeot 307 gasoline 2003 model.

Other objectives:

- Consolidation and expansion of programming skills on Mathematica software.

- Study of adsorption unit operation and its mathematical model taking into account the Transport Phenomena concepts.

- Make a 3D sketch of the 6-adsorption column system.

3. MATHEMATICAL MODEL

The model proposed by *Chatzopoulos & Varma (1995)* was the aqueous phase adsorption and desorption of toluene in activated carbon fixed bed adsorbers at 25ºC, investigated under a wide range of operating conditions. The model proposed two mass balances, for the fluid and the solid phase. These two balances are applied in our Faujasite 13X adsorption column.

The mathematical model used for a homogeneous particle considers two resistances to mass transfer:

- *External film resistance:* The film that surrounds the adsorbent resists the passage of matter between the fluid and the surface of the adsorbent.
- *Surface diffusion resistance* in the adsorbent particle.

The adsorption coefficient is not considered constant and depends on the concentration of the solute in the adsorbent, following an exponential function (see Eq.1).

$$D_s(q) = D_0\, e^{[k\left(\frac{q}{qsat}\right)]} \qquad (1)$$

Where D_0 is the surface coefficient when the adsorbate mass fraction in solid phase(q) is equal to zero (q=0) [cm^2/s], k is the experimental parameter [-] and q_{sat} is the adsorbate saturation mass fraction in solid phase [mg/g].

3.1. ADSORBATE MASS BALANCE FOR THE SOLID PHASE

Four conditions have been considered for the study of the adsorbent particle.

- Isothermal process.
- Monolayer adsorption (Langmuir isotherm).
- Adsorbent particle with spherical geometry.
- Fast adsorption kinetics.

Mass balance for one chemical specie in one differential volume (see Eq.2) contains four terms: term of non-stationary regime, convective term, dispersion term and generation term.

$$\frac{\partial \rho_s \, q}{\partial t} = \nabla . [\rho_s \, q \, v] = \nabla . \rho_s \, D_s \, \nabla q + G \qquad (2)$$

Where q is the adsorbate mass fraction [mg/g], D_s is the surface diffusion coefficient [cm^2/s], ρ_s is the apparent particle density [g/cm^3], G is the generation term of the species [$mg/(s \cdot m^3)$], v is the velocity [cm/s] and t is time in seconds.

Adsorbate mass balance for the solid phase contains the non-stationary term and the diffusion term, which allows the study of the variation in the solute concentration in function of the position of the particle and the time. Since in our case there is no reaction, the generation term is equal to zero and Eq.2 becomes Eq.3.

$$\frac{\partial \rho_s \, q}{\partial t} = \nabla . \rho_s \, D_s \, \nabla q \qquad (3)$$

The apparent particle density (ρ_s) is constant, so it remains as constant on both sides of the equation and can be removed. Besides, Eq.1 was incorporated in mass balance (see Eq.4) to take into account the variation of the diffusion coefficient at the surface (D_s).

$$\frac{\partial q}{\partial t} = \nabla . D_0 \, e^{[k\left(\frac{q}{qsat}\right)]} \, \nabla q \qquad (4)$$

Eq.4 is converted into spherical coordinates. Considering that the adsorbate concentration only depends on the radial position (r), the terms related to theta and phi do not contribute. The final balance is described by Eq. 5.

$$\frac{\partial q}{\partial t} = \frac{D_0}{r^2} \, \frac{\partial}{\partial r} \{ \, r^2 D_0 \, e^{[k\left(\frac{q}{qsat}\right)]} \, \frac{\partial q}{\partial r} \} \qquad (5)$$

The Langmuir isotherm (Eq.6) is used to relate the concentration in the solid phase and the gas phase.

$$q = \frac{q_{sat}\, b_L\, C_{in}}{1 + b_L\, C_{in}} \qquad (6)$$

Where b_L is the Langmuir isotherm parameter [cm^3/mg] and C_{in} [mg/cm^3] the initial concentration in the fluid phase.

Langmuir isotherm (Eq.6) is incorporated in the mass balance (Eq.5) obtaining Eq.7.

$$\frac{\partial q}{\partial t} = \frac{D_0}{r^2}\frac{\partial}{\partial r}\left\{ r^2 e^{\left[k\left(\frac{\frac{q_{sat}\, b_L\, C_p}{1 + b_L\, C_p}}{qsat} \right) \right]} \frac{\partial q}{\partial r} \right\} \qquad (7)$$

3.1.1. Initial conditions

- For Eq.7, at time zero, at all radius of the particle(r) and at all axial length of the bed (z), the adsorbate concentration remains at a fixed value.

$$t = 0, \qquad 0 \le r \le R, \qquad 0 \le z \le L$$

- The concentration in the solid phase is equal to zero.

$$q = 0 \qquad (7.1)$$

3.1.2. Boundary conditions

- For Eq.7, at all the time, at all axial length of the bed, there is not diffusion at r=0. At the centre of each zeolite particle there is a minimum of adsorbate mass fraction.

$$t > 0 \qquad 0 \le z \le L \qquad r = 0$$

$$\frac{\partial q}{\partial r}(r = 0) = 0 \qquad (7.2)$$

- All the time and at all axial length of the bed (z), the external mass transfer coefficient (k_f) is known and the following equality applies for r = R (at the surface of the zeolite 13X sphere particles):

$$D_0\,\rho_s\,e^{\left[k\left(\frac{q_{sat}\,b_L\,C_p}{1+b_L\,C_p}\right)\right]}\frac{\partial q}{\partial r}(r=R)=k_f(C-C_s) \qquad (7.3)$$

3.2. ADSORBATE MASS BALANCE FOR THE GAS PHASE

Initially, mass balance for one chemical specie in one differential volume (Eq. 8) is studied to describe the variation of the adsorbate concentration in the axial position (z) and the time (t). The balance is given by Eq. 8:

$$\varepsilon L\,\frac{\partial C}{\partial t}+\varepsilon L\,v_s\frac{\partial C}{\partial z}=\varepsilon L\,D_{eff}\frac{\partial^2 C}{\partial z^2}-(1-\varepsilon L)\,\frac{\partial q\,\rho_s}{\partial t} \qquad (8)$$

Where C is the solute liquid-phase concentration [mg/cm^3], D_{eff} is the dispersion coefficient [cm/s], vs is the superficial liquid velocity in bed [cm/s], εL is the bed void fraction [-] and (1- εL) is the bed fraction [-].

When the relationship between the bed length and the particle diameter is greater than 20 $(L/dp > 20)$, it can be considered that there is no axial solute dispersion in the bed so the dispersion term is removed of the equation, the generation term can be expressed as the difference between the adsorbate concentration in liquid-phase and the equilibrium concentration in the solid-liquid interface (see Eq.9), and the surface area of the particle has to be considered.

$$\frac{\partial C}{\partial t}=-\frac{v_s}{\varepsilon L}\frac{\partial C}{\partial z}-\frac{3}{R}\,\frac{(1-\varepsilon L)}{\varepsilon L}\,k_f\,(C-C_s) \qquad (9)$$

Where Cs is the equilibrium concentration in the solid-gas interface [mg/cm^3] and R is the radius of the adsorbent particle [cm].

3.2.1. Initial conditions

- For Eq.9, at time zero, at all radius of the particle(r) and at all axial length of the bed (z), the adsorbate concentration remains at a fixed value.

$$t = 0, \qquad 0 \le r \le R, \qquad 0 \le z \le L$$

- There is no CO_2 along the bed at the beginning of the adsorption.

$$C = 0 \qquad (9.1)$$

3.2.2. Boundary conditions

- For Eq.9, at all the time and at the beginning of the adsorption column (z = 0), the adsorbate concentration is equal to the adsorbate initial concentration in the gas phase:

$$t > 0 \qquad z = 0$$

$$C = C_{in} \qquad (9.2)$$

3.3. DIMENSIONLESS ADSORBATE MASS BALANCE

Following dimensionless quantities have been employed to develop the mathematical model of CO_2 adsorption process:

$$\rho = \frac{r}{R}; \quad \xi = \frac{z}{L}; \quad \tau = \frac{D_0\, t}{R^2}; \quad u = \frac{C}{C_{ref}}; \quad \eta = \frac{q}{q_{ref}};$$

$$Bi = \frac{k_f\, R\, C_{ref}}{\rho_s\, D_0\, q_{ref}}; \quad A = \frac{v_s\, R^2}{\varepsilon L\, D_0\, L}; \quad B = \frac{3\,(1-\varepsilon L)\, k_f\, R}{\varepsilon L\, D_0} \qquad (10)$$

Where ρ is the dimensionless radius particle[-], ξ is the dimensionless bed length[-], τ is the dimensionless time [-], u is the dimensionless gas concentration [-], η is the dimensionless solid concentration [-],Bi, A, B are dimensionless parameters, $C_{ref} = C_{in}$ [mg/cm^3], q_{ref} is the adsorbate mass fraction in equilibrium with C_{ref}[mg/g].

3.3.1. Dimensionless solute balance in solid phase

Applying the dimensionless parameters (Eq.10) in the solid mass balance (Eq.7), the dimensionless balance in solid phase (Eq.11) is obtained.

$$\frac{\partial \eta}{\partial \tau} = \frac{1}{\rho^2} \frac{\partial}{\partial \rho} \{\rho^2 \, e^{[k\left(\frac{\eta}{\eta_{sat}}\right)]} \frac{\partial \eta}{\partial \rho}\} \qquad (11)$$

Where η_{sat} is the η parameter when q is saturated.

Initial Conditions

- For Eq.11, at time zero, at all radius of the particle (ρ) and at all axial length of the bed (ξ), the adsorbate concentration remains at a fixed value.

$$\tau = 0, \qquad 0 \leq \rho \leq R, \qquad 0 \leq \xi \leq L$$

The concentration in the solid phase is equal to zero.

$$\eta = 0 \qquad (11.1)$$

Boundary Conditions

- During the adsorption process, at all axial length of the bed (ξ), there is not diffusion at ρ=0.

$$\tau > 0, \qquad 0 \leq \xi \leq 1, \qquad \rho = 0$$

$$\frac{\partial \eta}{\partial \rho}(\rho = 0) = 0 \qquad (11.2)$$

- All the time and at all axial length of the bed (ξ), the following equality applies for ρ = 1 (surface diffusion of the adsorbent):

$$e^{\left[k\left(\frac{\eta}{\eta_{sat}}\right)\right]} \frac{\partial \eta}{\partial \rho_{(\rho=1)}} = Bi \, (u - u_s) \qquad (11.3)$$

3.3.2. Dimensionless solute balance in gas phase

Applying the dimensionless parameters (Eq.10) in the gas mass balance (Eq.9), the dimensionless balance in gas phase (Eq.12) is obtained.

$$\frac{\partial u}{\partial \tau} = -A \frac{\partial u}{\partial \xi} - B \, (u - u_s) \qquad (12)$$

Initial Conditions

- At time zero, at all radius of the particle (ρ) and at all axial length of the bed (ξ), the adsorbate concentration in the gas phase remains equal to zero.

$$\tau > 0, \qquad 0 \le \rho \le 1, \qquad 0 \le \xi \le 1$$
$$u = 0 \qquad (12.1)$$

Boundary Conditions

- At all the time and at all the radius of the particle, the adsorbate concentration is equal to adsorbate initial concentration in gas phase at the beginning of the adsorption column.

$$\tau > 0, \qquad \xi = 0, \qquad 0 \le \rho \le 1,$$
$$C = C_{in} \qquad (12.2)$$

The model implemented in Mathematica are Eq. 11 and its initial and boundary conditions to describe the mass transfer at the zeolite particles and the Eq. 12 and its initial and boundary conditions to describe the mass transfer in the gas phase along the bed. The implementation in Mathematica is presented in the next chapter.

4. ADSORPTION SIMULATION CODE IN MATHEMATICA

Two codes were implemented, one based on the discretization of the equations according my Transport Phenomena class notes, and one used by Exposito (2019) in his TFM using other statements.

The first discretized option code (see Appendix 2), required a very fine mesh to obtain reliable results that must be performed using a computer power that cannot be attained by my current personal computer. I have been working also on using an IQTC Linux supercomputer or to use the recent UB acquired MATLAB software instead of Mathematica to speed up the computation. However, these options to speed up the computation are out the scope of the present study and will be performed as future work. Hence, the results presented in this work are according to the second code which has been extended, depurated, improved and applied to simulate the adsorption of exhaust gases from cars operating close to real conditions. Some results were not viable but the operation conditions providing consistent results have been determined. The study is in the framework of a project effectuated at the IQTC and according the results obtained, and an Engineering Company participating in the project has proposed me to continuate working with them in the project as student in practice.

4.1. ADSORPTION PARAMETERS

The different parameter values employed to simulate the CO_2 adsorption column are shown in Table 6 and 7.

Table 6. Adsorption constant parameters.

COLUMN PARAMETERS	
Column length = bed length [cm]	55
Column diameter = bed diameter [cm]	25
Interparticle void fraction, ε [-]	0,2576
ADSORBED PARAMETERS	
Surface diffusion coefficient at q=0, D_0 [cm^2/s]	$5 \cdot 10^{-7}$
Experimental Constant, k[-]	3,2
ZEOLITE 13X PARAMETERS	
Particle density, ρs [g / cm^3]	1,05
Particle Diameter [cm]	0,03
LANGMUIR ISOTHERM PARAMETERS (CO_2)	
$Bi_{,0}$ [m^3/mol]	$8,65 \cdot 10^{-7}$
ΔU [J/mol]	$-3,61 \cdot 10^{-4}$
Temperature [K]	313
CO_2 mass fraction saturation in the adsorbent, q_{sat} [mg/g]	137,2
GAS PARAMETERS	
CO_2 density at 1 bar, 40ºC, ρ_{CO2} [g/cm^3]	$1,75 \cdot 10^{-3}$
N_2 density at 1 bar, 40ºC, ρ_{N2} [g/cm^3]	$1,11 \cdot 10^{-3}$
$H_2O(v)$ density at 1 bar, 40ºC, ρ_{H2O} [g/cm^3]	$5,12 \cdot 10^{-5}$
CO2 dynamic viscosity at 1 bar, 40ºC, μ_{CO2} [g/cm·s]	$1,45 \cdot 10^{-4}$
N_2 dynamic viscosity at 1 bar, 40ºC, μ_{N2} [g/cm·s]	$1,80 \cdot 10^{-4}$
$H_2O(v)$ dynamic viscosity at 1 bar, 40ºC, μ_{H2O} [g/cm·s]	$1,03 \cdot 10^{-4}$

The constant parameters have been mainly obtained by experimental data of a CO_2 adsorption on a Zeolite 13X column, bibliographical sources and some considerations that are discussed in the following paragraphs.

- **Surface diffusion coefficient at q=0, D_0:** This value is between the range of 10^{-8}-10^{-9} cm^2/s according to *Kouichi et al (2006)*, and the value $5 \cdot 10^{-7}$ has been considered. It is responsible for the passage of the molecules through the adsorbent, the higher this coefficient, the easier it is for the particles to pass through and saturate earlier.
- **Experimental constant, k [-]:** The value of this parameter is usually between 0 and 5. Setting 0 when the superficial diffusivity (D_s) is constant (See Eq.1).
- **Volumetric gas flow, Q [cm^3/s]:** The output flow depends on the car model, since it depends on its displacement and on the revolutions per minute at which the vehicle is going. For this reason, I have chosen the Peugeot 307 (2001-2005 model) as a reference, because I have a reliable source of data.

  The car has 4 cylinders, with a displacement of 1587 cm^3, with 2500 rpm if good use of the gears is made. It is known that for 2 revolutions there is an exhaust, which means that every 2 revolutions, the gas that occupies the volume of each cylinder goes out. Therefore, the flow is equal to the volume of the displacement multiplied by half the number of revolutions per minute *(Espada García)*, seen in Eq. 13.

$$Q = 1587 cm^3 \cdot 2500 \frac{rev}{min} \cdot \frac{1\ min}{60\ s} \cdot \frac{1\ exhaust}{2\ rev} = 1587 \cdot \frac{41.67}{2}$$

$$Q = 33062.5\ \frac{cm^3}{s} \qquad (13)$$

- **Superficial velocity, vs [cm/s]:** It has been obtained by the following equation (Eq.14).

$$vs = \frac{Q}{\varepsilon L\ \pi\ (\frac{dc}{2})^2} = \frac{33062.5 \frac{cm^3}{s}}{0{,}2576\ \pi\ (\frac{25}{2})^2 cm^2} = 261.47 \frac{cm}{s} \qquad (14)$$

- **CO2 initial concentration, C_{in} [mg CO_2/cm^3]:** The Peugeot 307 has a consumption of 7.5L per 100km, using the gasoline emission factor of 2.196 kg CO_2/L *(Gobierno de España, 2018)* you can know the g of CO_2 per km emitted. Likewise, the concentration depends on the speed at which the vehicle is going and its revolutions (included in the flow).

$$\text{Cin} = \frac{7{,}5\ \text{l}}{100\ \text{km}} \cdot \frac{2{,}196\ \text{kg CO}_2}{1\ \text{l}} \cdot \frac{1000\ \text{g}}{1\ \text{kg}} \cdot \frac{80\ \text{km}}{\text{h}} \cdot \frac{1\ \text{h}}{3600\ \text{s}} \cdot \frac{1\ \text{s}}{33062{,}5\ \text{cm}^3} \cdot \frac{1000\ \text{mg}}{1\ \text{g}} =$$

$$\text{Cin} = 0.111\ \frac{\text{mg CO}_2}{\text{cm}^3} \qquad (15)$$

- **CO_2 volume fraction [cm^3 CO2/cm^3 mixture]:** It depends on the speed and revolutions of the vehicle; it is calculated using the following formula (Eq.16):

$$\frac{7{,}5\ \text{l}}{100\ \text{km}} \cdot \frac{2{,}196\ \text{kg CO}_2}{1\ \text{l}} \cdot \frac{1000\ \text{g}}{1\ \text{kg}} \cdot \frac{80\ \text{km}}{\text{h}} \cdot \frac{1\ \text{h}}{3600\ \text{s}} \cdot \frac{1\ \text{cm}^3\text{CO}_2}{0.001754\ \text{g CO}_2} = 2086.66 \frac{cm^3 CO_2}{s}$$

$$\text{CO}_2\ \text{volume fraction} = \frac{2086.66 \frac{\text{cm}^3\text{CO}_2}{\text{s}}}{33062.5\ \frac{\text{cm}^3\text{mixture}}{\text{s}}} = 0.0631 = 6.31\% \sim \mathbf{6} \qquad (16)$$

- **CO_2 mass fraction [g CO2/g mixture]:** It has been calculated using the following approximated composition (Table 7) to calculate the average molecular mass (see Eq.17) and the mass fraction of the gases (see Eq.18).

Table 7. Approximated composition of exhaust gases

Composition	%Vol.	ρ [g/cm^3]	μ[g/cm·s]
CO_2	6	1,75E-03	1,45E-04
N_2	79	1,09E-03	1,80E-04
H_2O	15	1,09E-03	1,80E-04

$$\text{Mmixture} = 0.06\ \text{M}_{\text{CO2}} + 0.79\ \text{M}_{\text{N2}} + 0.15\ \text{M}_{\text{H2O}} \qquad (17)$$

$$\mathbf{Mmixture} = 0.06 \cdot 44 + 0.79 \cdot 28 + 0.15 \cdot 18 = \mathbf{27.46}\ \frac{\mathbf{g\ mixture}}{\mathbf{mol\ mixture}}$$

$$\mathrm{i}_{\text{ mass fraction }} = \mathrm{i}_{\text{ volume fraction }} \cdot \frac{\mathrm{M_i}(\frac{\mathrm{g}}{\mathrm{mol}})}{\mathrm{M_{mixture}}(\frac{\mathrm{g}}{\mathrm{mol}})} \qquad (18)$$

$$\mathbf{CO_2\ mass\ fraction} = 0.06 \frac{\text{mol } CO_2}{\text{mol mixture}} \cdot \frac{44 \text{ g } CO_2}{1 \text{ mol } CO_2} \cdot \frac{1 \text{ mol mixture}}{27.46 \text{ g mixture}} = \mathbf{0.096}$$

$$\mathbf{N_2\ mass\ fraction} = 0.79 \frac{\text{mol } N_2}{\text{mol mixture}} \cdot \frac{28 \text{ g } N_2}{1 \text{ mol } N_2} \cdot \frac{1 \text{ mol mixture}}{27.46 \text{ g mixture}} = \mathbf{0.81}$$

$$\mathbf{H_2O_{mass\ fraction}} = 0.15 \frac{\text{mol } H_2O}{\text{mol mixture}} \cdot \frac{18 \text{ g } H_2O}{1 \text{ mol } H_2O} \cdot \frac{1 \text{ mol mixture}}{27.46 \text{ g mixture}} = \mathbf{0.098}$$

The gas density, ρ_{gas} and gas viscosity μ_{gas} have been obtained by the equations Eq.19 and Eq.20.

$$\rho_{\text{gas}} = \rho_{\text{CO2}} \cdot \mathrm{CO}_{2\text{ mass fraction}} + \rho_{\text{N2}} \cdot \mathrm{N}_{2\text{ mass fraction}} + \rho_{\text{H2O}} \cdot \mathrm{H_2O_{mass\ fraction}} \qquad (19)$$

$$\rho_{\text{gas}} = 1.175\ 10^{-3} \cdot 0.096 + 1.109\ 10^{-3} \cdot 0.81 + 5.12\ 10^{-5} \cdot 0.098$$

$$\boldsymbol{\rho_{gas} = 5.31 \cdot 10^{-4} \frac{g}{cm^3}}$$

$$\mu_{\text{gas}} = \mu_{\text{CO2}} \cdot \mathrm{CO}_{2\text{ mass fraction}} + \mu_{\text{N2}} \cdot \mathrm{N}_{2\text{ mass fraction}} + \mu_{\text{H2O}} \cdot \mathrm{H_2O_{mass\ fraction}} \qquad (20)$$

$$\mu_{gas} = 1.45\ 10^{-3} \cdot 0.096 + 1.80\ 10^{-3} \cdot 0.81 + 1.03\ 10^{-5} \cdot 0.098$$

$$\boldsymbol{\mu_{gas} = 8.41 \cdot 10^{-5} \frac{g}{cm \cdot s}}$$

- **External mass transfer coefficient, Kf:** Has been calculated using Eq.21. *(Delgado et al, 2014)*

$$\mathrm{kf} = \frac{\mathrm{vs}}{\varepsilon \mathrm{L} \cdot \mathrm{Sc}^{2/3}} \cdot \left(\frac{0.765}{\mathrm{Re}^{0.82}} + \frac{0.365}{\mathrm{Re}^{0.386}} \right) \qquad (21)$$

$$\mathrm{kf} = \frac{261.47}{0.2576 \cdot 1.14^{\frac{2}{3}}} \cdot \left(\frac{0.765}{41255^{0.82}} + \frac{0.365}{41255^{0.386}} \right)$$

$$\mathbf{kf = 5.73}$$

Where Sc is the Schmidt number for theCO_2/air mixture (similar to our exhaust gas mixture) and Re is the Reynolds number, obtained by Eq.22:

$$\mathbf{Re} = \frac{dc \cdot vs \cdot \rho_{mixture}}{\mu_{mixture}} = \frac{25\ cm \cdot 261.47\ \frac{cm}{s} \cdot 5.31\ 10^{-4} \frac{g}{cm^3}}{8.41\ 10^{-5} \frac{g}{cm \cdot s}} = \mathbf{41255} \qquad (22)$$

- **Langmuir isotherm constant, b_L[mg CO_2/cm³]:** Its value has been obtained by the following equation (Eq.23).

$$b_L = b_{i,0} \cdot e^{\left(\frac{-\Delta U}{R\,T}\right)} \qquad (23)$$

$$b_L = 8{,}65 \cdot 10^{-7} \left[\frac{m^3}{mol}\right] * \frac{10^6 cm^3}{1\ m^3} * \frac{1 mol\ CO2}{44\ g\ CO2} * \frac{1g}{1000\ mg} * Exp\left(\frac{\Delta U \left[\frac{J}{mol}\right]}{8{,}314 \left[\frac{J}{K\ mol}\right] * 313[K]}\right)$$

$$\mathbf{b_L = 35\ \frac{mg\ CO_2}{cm^3}}$$

4.2. RESOLUTION OF THE MATHEMATICAL MODEL

Data

```
Needs["NDSolve`FEM`"]
cilindrada = 1587; revoluciones = 2500 / 60;
revporcilindro = revoluciones / 2;
Q = cilindrada revporcilindro; litrosconsumo = 7.5 / 100;
gramoporkm = 2.196 litrosconsumo 1000 ; velocidad = 80;
cin = gramoporkm velocidad 1000 / (3600 Q); dp = 0.03; Rr = dp / 2;
dc = 25; ρs = 1.05; k = 3.2; Ds = 5 × 10^-7; εL = 0.2576;
Zz = 55; vs = Q / (εL Pi (dc^2) / 4);
Mass = 0.06 × 44 + 0.78 × 28 + 0.15 × 18 + 1 × 28;
CO2mf = 0.06 44 / Mass; N2mf = 0.78 28 / Mass;
H2Ovmf = 0.15 18 / Mass; COmf = 0.01 28 / Mass;
ρCO2 = 1.754 × 10^-3; ρN2 = 1.109 × 10^-3;
ρCO = 1.109 × 10^-3; ρH2Ov = 0.0512 × 10^-3;
μCO2 = 1.45 × 10^-4; μN2 = 1.80 × 10^-4;
μCO = 1.80 × 10^-4; μH2Ov = 1.03 × 10^-4;
ρgas = CO2mf ρCO2 + N2mf ρN2 + H2Ovmf ρH2Ov + COmf ρCO;
μgas = CO2mf μCO2 + N2mf μN2 + H2Ovmf μH2Ov + COmf μCO;
Reynolds = dc vs ρgas / μgas;
kf = vs / (εL 1.14^(2 / 3)) (0.765 / Reynolds^0.82 + 0.365 / Reynolds^0.386);
qsat = 137.2;
bio = 8.65 × 10^-7; ΔU = -36641.21; R = 8.134; T = 313;
bl = bio Exp[-ΔU / (R T)] 10^6 / 44000;
qref = bl cin qsat / (1 + bl cin);
nsat = qsat / qref;
bi = kf Rr cin / (ρs Ds qref);
A = vs Rr^2 / (εL Ds Zz);
B = 3 (1 - εL) kf Rr / (εL Ds);
```

Mesh

```
mesh = ToElementMesh[Rectangle[{0, 0}, {1, 1}], "MaxCellMeasure" → 0.0005]
mesh["Wireframe"]
```

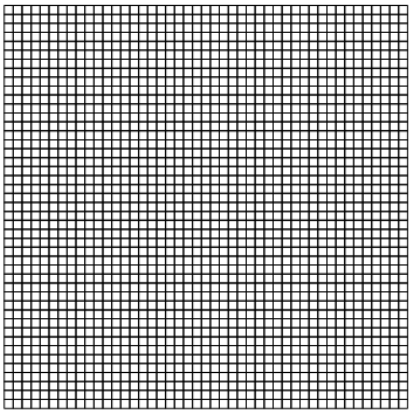

To make the mesh of our adsorption column, dimensionless radius of the zeolite 13X particle and the length of the column have been employed, using values between 0 and 1.

- Being 0 for the beginning of the column or centre of the particle.
- Being 1 for the outlet of the column or external surface of the particle.

By this way, the resolution of the simulation is simplified, the mesh becomes a square with sides compressing between 0 and 1. If no dimensionless values were employed, it would get much harder to mesh the column due to the different scale of the axis.

To create the mesh in Mathematica®:

"NDSolve'FEM" option has to be activated, which is deactivated by default.

"ToElementMesh", creating a 0 to 1 side square and specifying the cell measure we want (the smaller this value is, the greater number of nodes and accuracy). A value of 0,0005 maximum cell measure has been specified to create the mesh, generating 2025 elements, 45 elements per row.

Iteration (time steps) resolution

```
At = 3*10^-4;
n = 6500;
i = 0;
Monitor[Do[i++; If[At < 3*10^-4, At = At + 1*10^-5, At = 3*10^-4]; csol = NDSolveValue[{neq1, bc2}, c, {x, z} ∈ mesh];
 monitor  repite  si                                                  valor de resolución diferencial numérica

  eq = (q[x, z] - q1[x, z]) / At - 1 / x^2  D[1 * x^2 * Exp[k q1[x, z] / nsat] * (D[q[x, z], x]), x] ==
                                            deriva      exponencial                 deriva
    NeumannValue[0, x == 0] + NeumannValue[bi (c1[x, z] - cs[x, z]) / ( Exp[ k q1[x, z] / nsat]), x == 1];
     valor Neumann                 valor Neumann                        exponencial

  neq = (c[x, z] - c1[x, z]) / At + A (D[c[x, z], z]) + B (c[x, z] - cs[x, z]) == 0;
                                      deriva

  qsol = NDSolveValue[{eq3}, q, {x, z} ∈ mesh];
         valor de resolución diferencial numérica

  solutions = Append[solutions, {qsol, csol}];
              añade

  qplot = Append[qplot, Plot[qsol[x, 1], {x, 0, 1}]];
          añade          representación gráfica

  cplot = Append[cplot, Plot[csol[1, z], {z, 0, 1}]];
          añade          representación gráfica

  neq1 = neq /. {cs[x, z] → -((qsol[x, z] * qref) / (bl (qsol[x, z] * qref - qsat) * cin)), c1[x, z] → csol[x, z]};
  eq3 = eq /. {q1[x, z] → qsol[x, z], q1^(1,0)[x, z] → D[qsol[x, z], x],
                                                       deriva

    c1[x, z] → csol[x, z], cs[x, z] → -((qsol[x, z] * qref) / (bl (qsol[x, z] * qref - qsat) * cin))}, n], i]
```

The mathematical model explained has been resolved along the mesh generated.

By using the function “Monitor”, the program shows the iteration number that is resolving at that moment.

A conditional has been employed during the iterations to establish an inflation in the time to enhance the accuracy at the beginning of the process, increasing the time step on each iteration. It is necessary in some cases in which at the beginning of the adsorption there are some drastic changes and the time steps needs to be very small. By using an inflation in the time, convergence is enhanced, and the code is improved, being necessary less iterations that if no inflation is considered.

Axial dispersion has been considered negligible, consequently, at the same length point, the solid particles of the bed are equally mass balanced. Hence, when a particle at one point is saturated, the other particles at the same point are also saturated, being possible to simulate only one particle at each point of length to know the adsorption behaviour inside the adsorbent.

Boundary and initial conditions have been specified by two different ways:

- "Dirichlet Condition" has been employed when the condition is just an expression equalized to some term.
- "Neumann Value" must be used when the condition is an expression containing a derivative term, allowing to specify the value of the derivative at some point of the variable.

Equations of the mathematical code are resolved iterating n times for a differential of time(Δt), solving the equations using "NDSolveValue" function on each iteration.

- "eq" variable is the equation of CO_2 concentration at solid phase and its initial conditions have been specified on "eq3".
- "neq" variable is the equation of CO_2 concentration on gas phase and its initial conditions have been specified on "neq1".

Solutions plotted for solid and gas phase

```
ContourPlot[qsol[x, z], {x, 0, 1}, {z, 0, 1}, PlotRange → All, PlotLegends → Automatic]
Plot3D[qsol[x, z], {x, 0, 1}, {z, 0, 1}, PlotRange → All]
Plot[qsol[x, 1], {x, 0, 1}, PlotRange → All]
Plot[qsol[x, 3 / 4], {x, 0, 1}, PlotRange → All]
Plot[qsol[x,1/2],{x,0,1},PlotRange→All]
ContourPlot[csol[x,z],{x,0,1},{z,0,1},PlotLegends→Automatic]
Plot3D[csol[x,z],{x,0,1},{z,0,1}]
Plot[csol[1,z],{z,0,1}]
ListAnimate[qplot]
ListAnimate[cplot]
```

List Animate solution for solid and gas phase

```
contours = {}
plotc = {}
i = 0;

Do[i = i + 10; contours = Append[contours, ContourPlot[solutions[[i]][[1]][x / 0.15, z / 55],
repite                                añade                representación de contornos
    {x, 0, 0.15}, {z, 0, 55}, PlotRange → All, PlotLabel → {"time in s" (At i Rr^2) / Ds},
                                  rango de rep···  todo  etiqueta de representación
    PlotLegends → Automatic, FrameLabel → {"x [mm]", "z [cm]" },
    leyendas de rep···  automático  etiqueta de marco
    Contours → {0, 0.1, 0.2, 0.3, 0.4, 0.5, 0.6, 0.7, 0.8, 0.9, 0.99}]],
    contornos
 Dimensions[solutions][[1]] / 10]
 dimensiones
i = 0;
Do[i++; plotc = Append[plotc, Plot[solutions[[i]][[2]][1, z / 55],
repite                añade              representación gráfica
    {z, 0, 55}, AxesLabel → {"z [cm]", "C/Co [-]"},
                  etiqueta de ejes
    Ticks → Automatic, PlotRange → {{0, 55}, {0, 1.1}},
    marcas  automático  rango de representación
    PlotLabel → {"time in s" (At i Rr^2) / Ds}]], Dimensions[solutions][[1]]]
    etiqueta de representación                  dimensiones


ListAnimate[contours]
anima lista
ListAnimate[plotc]
anima lista
```

To improve the vision of the evolution of the concentration on each point of the column in the gas and solid phase at any time, an animated graphic has been used in both. For the solid phase, the contours of the dimensionless concentrations have been represented with a jump of 0.1. The dimensionless time has been converted to time in seconds in order to study better the results.

5. RESULTS

5.1. INITIAL RESULTS

First, an attempt was made to carry out the simulation with the particle diameter data provided (0.201 cm) by changing the column diameter to adapt it to the flow rate of the exhaust gases from vehicles.

5.1.1. Adsorbate concentration on solid phase

Axial dispersion has been considered negligible, consequently, at the same length point, the solid particles of the bed are equally mass balanced. Hence, when a particle at one point is saturated, the other particles at the same point are also saturated, being possible to simulate only one particle at each point of length to know the adsorption behaviour inside the adsorbent.

The x-axis represents the radius of the particle in mm, and the y-axis represents the height of the column in cm. The particle begins to saturate by the surface since it is the one that is in contact with the gas phase, as time passes the CO_2 reaches the interior of the particle.

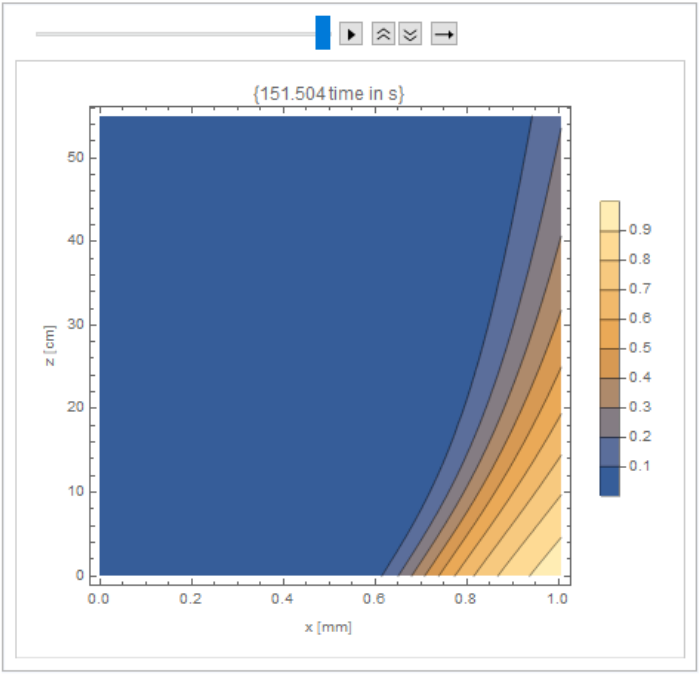

Figure 9. Dimensionless CO_2 concentration on solid phase at breaking point, t = 152 s.

It can be observed the CO_2 concentration inside the Faujasite 13X in function of the position in the column (z) and the radius of the particle (x) at different times.

The trend is not as expected, since at the breaking point the particles should be completely saturated at the entrance of the column and almost saturated at the exit. Instead it can be observed that in the entire column, no particle is completely saturated, only near the surface.

5.1.2. Adsorbate concentration on gas phase

The x-axis represents the length of the column, and the y-axis the dimensionless concentration from 0 to 1. The breaking time is the one in which the concentration at the exit of the column is 0.05.

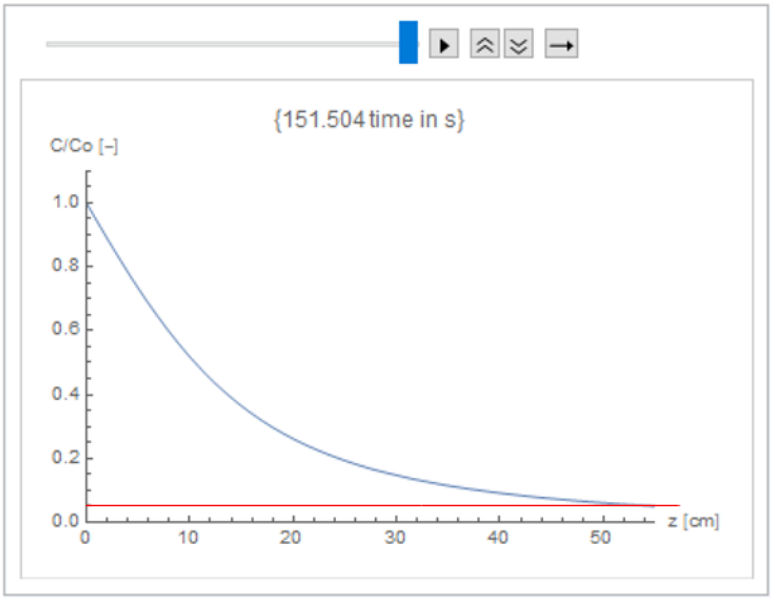

Figure 10. Dimensionless CO_2 concentration on gas phase at breaking point, t = 152 s.

5.2. CHANGES IN PARTICLE DIAMETER

Seeing that the particle was not saturated due to the high speed carried by the gas (because of the high flow rate), and there was less time for the exchange of matter on the surface of the solid, it was tried to decrease the diameter of the Faujasite 13X to that with the same speed the particle becomes saturated.

To determine when a particle diameter is viable, the matter transfer zone must be studied. It was tried to keep the strip as small as possible so that the particles in that zone are completely saturated before moving on to the next zone, thus obtaining a good column performance. This can be verified by looking at the graphic representation of the gas concentration along the column.

Particle diameter equal to 0.5 mm

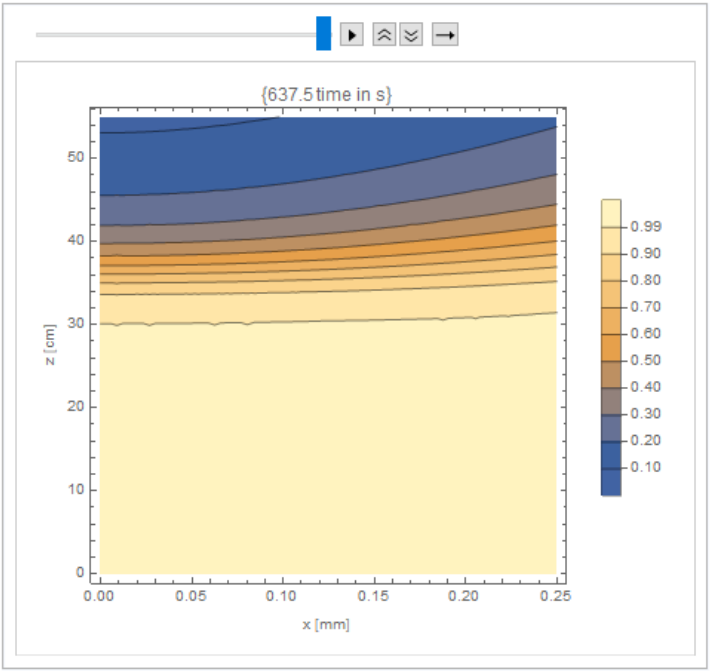

Figure 11. Dimensionless CO_2 concentration on solid phase at breaking point, t = 638 s.

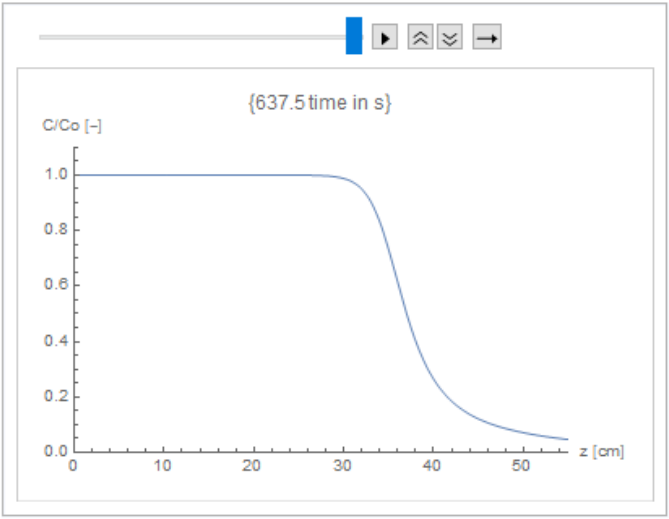

Figure 12. Dimensionless CO_2 concentration on gas phase at breaking point, t = 638 s.

Particle diameter equal to 0.3 mm

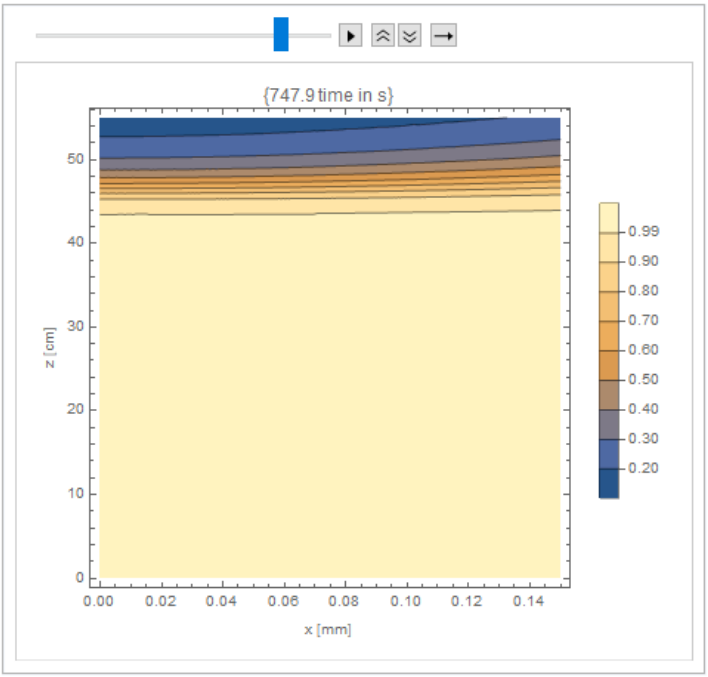

Figure 13. Dimensionless CO_2 concentration on solid phase at breaking point, t = 748 s.

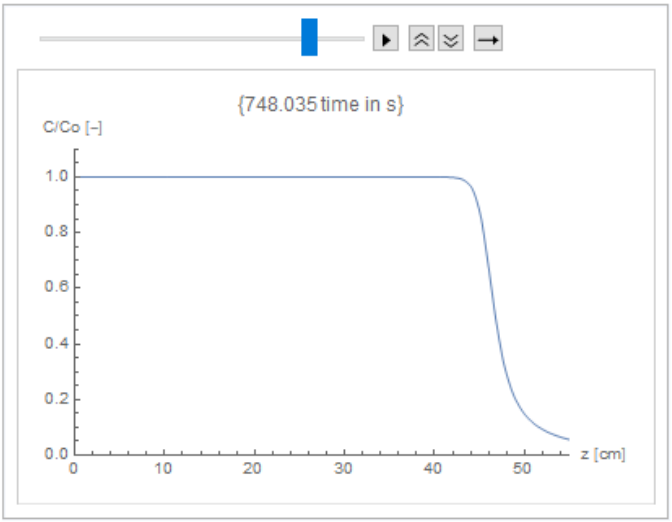

Figure 14. Dimensionless CO_2 concentration on gas phase at breaking point, t = 748 s.

At breaking point, the mass transfer zone is smaller, since the curve has a steeper slope and the zone with C / Co = 1 is longer. Throughout the column the particles are fully saturated at a higher height (45 cm) than the column with a diameter of 0.5 mm (30 cm).

The relationship between the diameter of the column and the breaking time according to the diameter of the particle has also been studied (see Appendix 1).

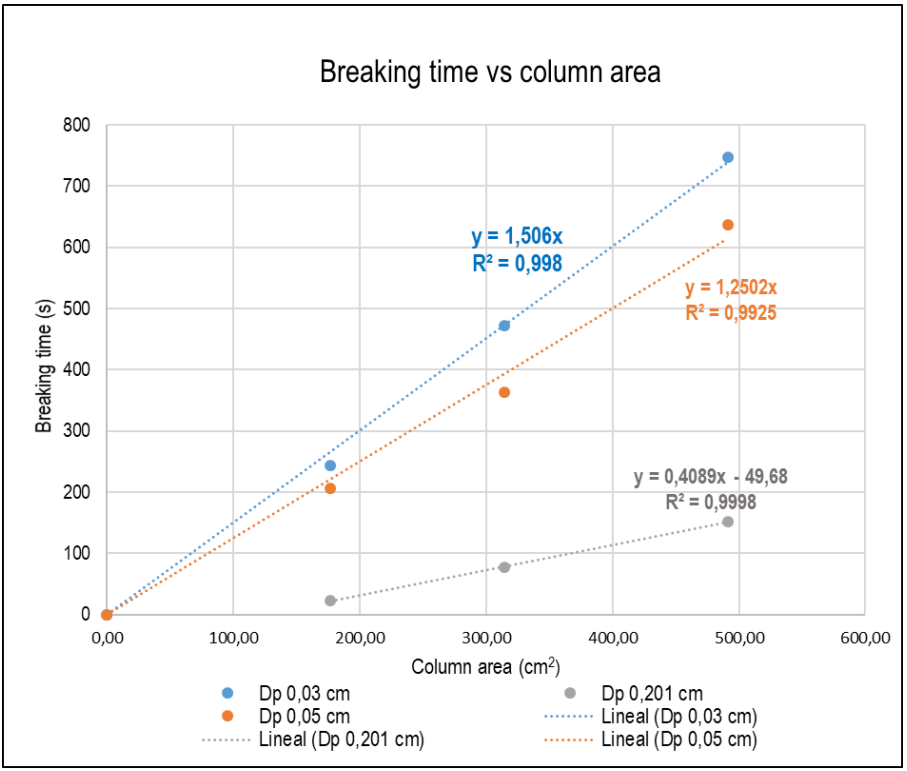

Figure 15. Trend depending on particle and column diameter.

For all particle diameters, the larger the column diameter, the higher the breakdown time as expected. After studying the initial particle diameter and seeing that it was not feasible, two smaller particle diameters were studied and compared with each other. In the range of the column diameter studied, both particle diameters follow a linear trend, however the particle with a diameter of 0.03 cm has a greater slope and therefore, for the same column diameter, it obtains a larger breaking time. Besides, the column is saturated at a higher height than the 0.05 cm particle diameter.

It is necessary to look for the particle diameter for which, at breaking time, most of the column is saturated. For this reason, the particle chosen to perform the simulation is the particle with a diameter of 0.03 cm. The diameter column chosen will be chosen later depending on the size of the car boot.

5.3. CHANGES IN TEMPERATURE

The relationship between temperature and breaking time has been studied for the chosen particle diameter (0.03 cm) and a constant column diameter of 25 cm.

Temperature equal to 40ºC (see the section above).

Temperature equal to 60ºC

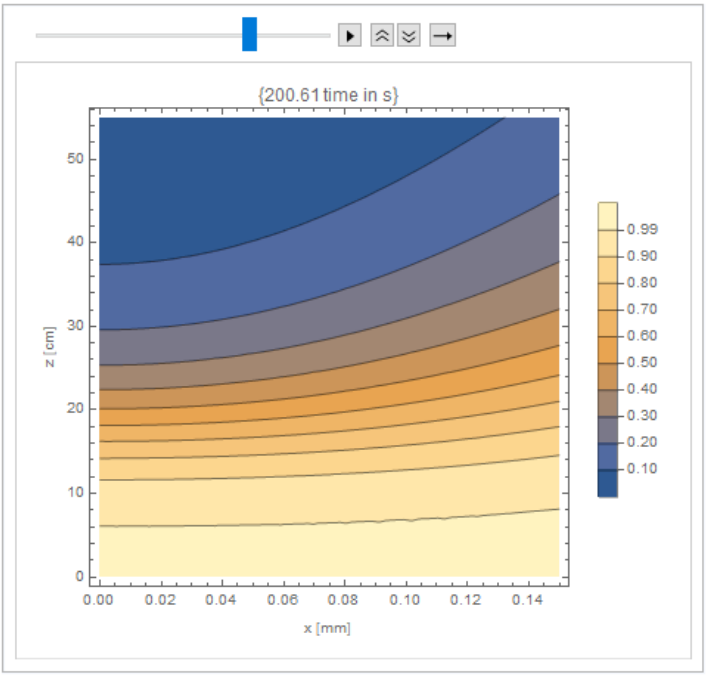

Figure 16. Dimensionless CO_2 concentration on solid phase at breaking time, t =201 s.

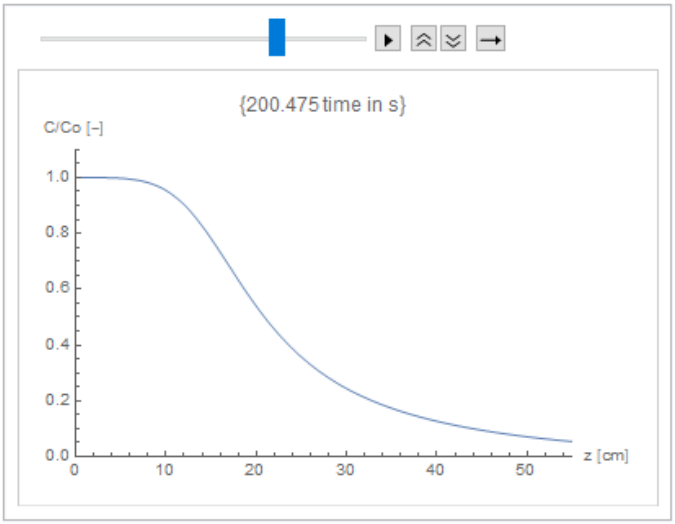

Figure 17. Dimensionless CO_2 concentration on gas phase at breaking time, t = 200 s.

Temperature equal to 80ºC

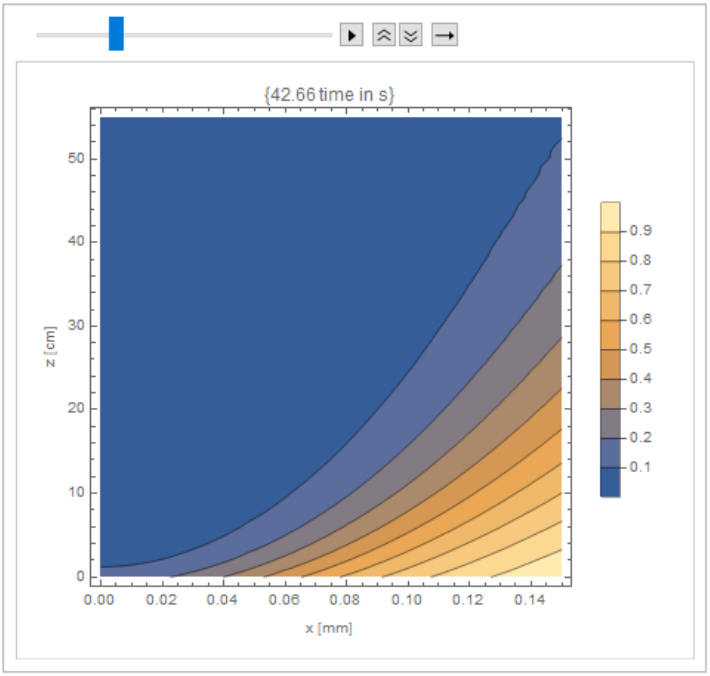

Figure 18. Dimensionless CO_2 concentration on solid phase at breaking point, t =43 s.

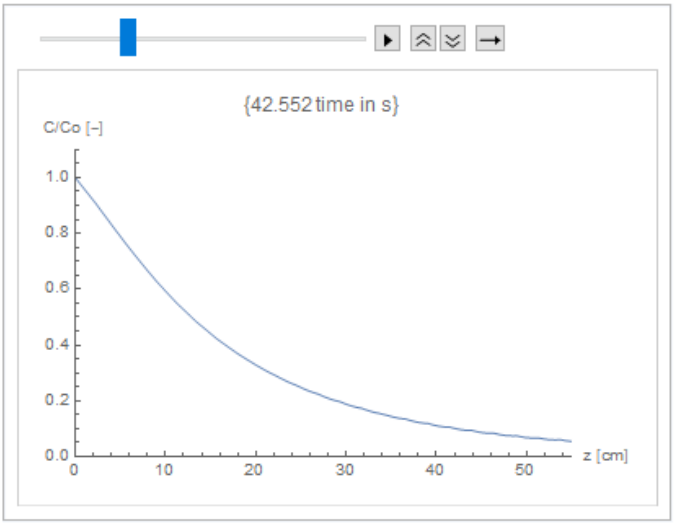

Figure 19. Dimensionless CO_2 concentration on gas phase at breaking point, t =43 s.

Table 8. Breaking time depending on temperature.

Temperature (ºC)	Breaking time (s)
40	748
60	200,5
80	42,6

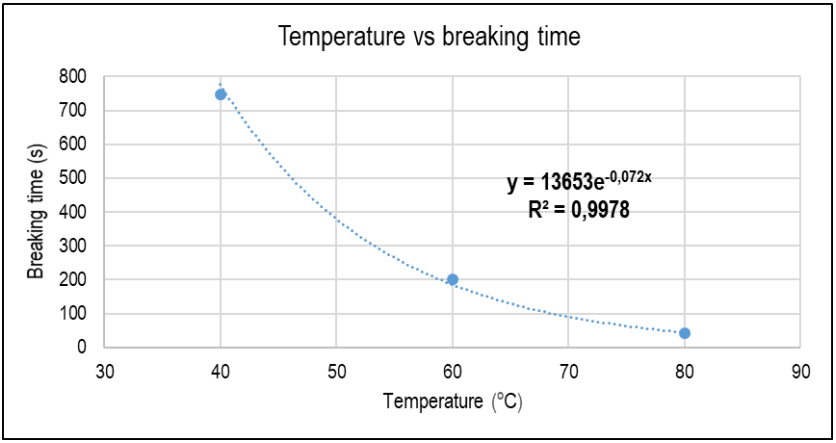

Figure 20. Exponential trend.

The trend is exponentially decreasing, therefore, when the temperature rises, the breaking time decreases significantly, for 60 degrees it still follows the expected trend moderately, while for 80 degrees practically does not capture CO_2. This confirms that adsorption is favoured at low temperatures.

5.4. NUMBER OF COLUMNS BASED ON BOOT SIZE

The car boot has measures of:

- 100 cm width
- 55 cm height
- 62 cm depth

The number of columns that fit in the boot have been calculated according to the diameter used and obtain the overall breaking time of each one to see which one provides a longer time.

Table 9. Total time depending on column diameter and number.

Column diameter(cm)	Breaking time (s)	Column number	Total time (s)
15	243	18	4374
20	472,5	8	3780
25	**748**	**6**	**4488**

Total time (min)	Total time (h)	km travelled	kg CO_2 captured
72,9	1,215	97,2	16,01
63,00	1,05	84,00	13,83
74,80	**1,25**	**99,73**	**16,43**

The best combination obtained is the 25 cm diameter column using a 6-column structure, obtaining an hour and a quarter of autonomy and preventing 16.4 kg of CO2 from being emitted into the atmosphere.

To see an outline of how the columns would look inside the boot, a perspective model has been made with the 3DS Max program, and the front elevation, plan and side elevation with the AutoCAD program.

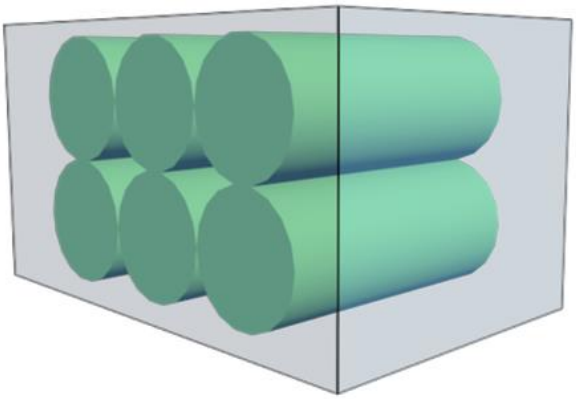

Figure 21. 3D perspective of the 6-column structure inside the boot.

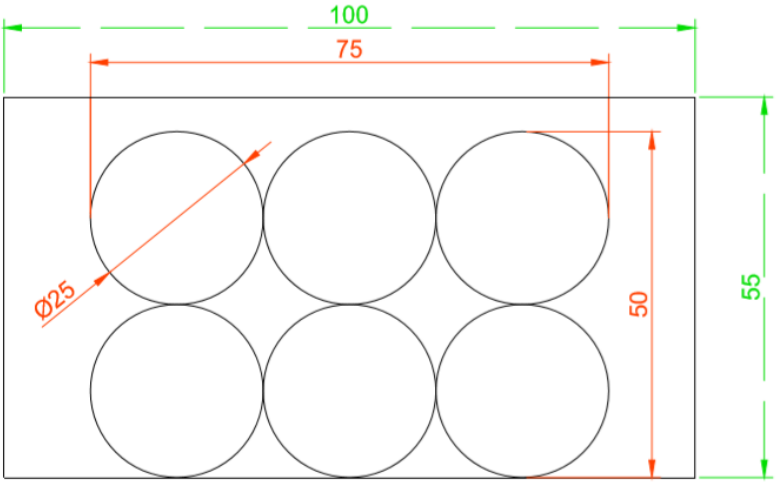

Figure 22. Front elevation of the 6-column structure inside the boot.

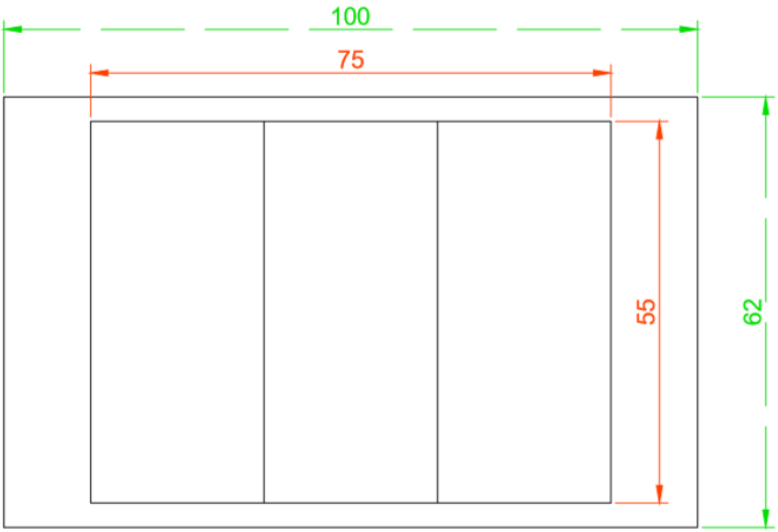

Figure 23. Plan view of the 6-column structure inside the boot.

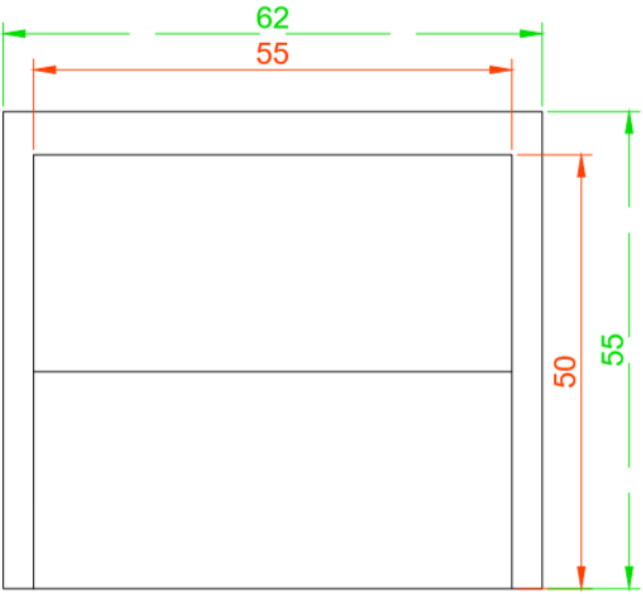

Figure 24. Side elevation of the 6-column structure inside the boot.

6. CONCLUSIONS

A CO_2 adsorption column model has been implemented and simulated using Mathematica and analysed for different input parameter values (see Appendix 1). For the best values found, the following conclusions have been determined.

- The CO_2 adsorption inside the Faujasite 13X particles can be simulated for the composition of exhaust gases from vehicles and has been represented at different times along the column and shown in function of the radius particle, from the external surface to the centre.
- The most suitable particle diameter is 0.03 cm and 25 cm of column diameter, with a structure of 6 columns, providing the higher total time.
- CO_2 concentration on gas phase along the column has been represented, obtaining values of this concentration with time. A total time of 12.47 min (748 s) per adsorption column until the breaking point is reached has been obtained. Therefore, the total time of the 6-column structure is 75 min, an hour and a quarter.
- The 6-column structure prevents the emission of 16.4 kg of CO_2 into the atmosphere.

7. FUTURE WORK

During the realization of this work, the following proposals emerged, which should be considered for the continuation of the study:

- Realization of the experimental part, obtaining input parameter values that may differ from those employed (i.e. external mass transfer coefficient and experimental value "k").
- Simulate the desorption process to study the regeneration of the column by raising up the temperature (TSA) or reducing the pressure (VSA).
- Use a larger column for vehicles without the restriction of the boot size so that the surface speed follows the heuristics.
- Apply the program to solve columns applied to ship and plain engines.
- Use a more powerful processor if more simulation precision is desired, increasing the resolution speed allowing us to reduce the time step and heighten the mesh nodes.

REFERENCES AND NOTES

- Baerlocher, Lynne, McCusker & Olson (1995). Atlas of zeolite framework types. Sixth edition (2007), Volume 15, Issue 5, 439 – 443.
- Chatzopoulos, D. & Varma, A. Aqueous phase adsorption and desorption of toluene in activated carbon fixed beds: Experiments and model. Chemical Engineering Science, Volume 50, Issue 1, 1995, pages 127-141.
- Chemical Structure[in-line]. Faujasite Structure.
  URL adress: <https://chemicalstructure.net/portfolio/faujasite/> [15/04/20].
- Chowdhury, Z. Z., Hamid, S. B. A. & Zain, S. M. (2015). Evaluating design parameters for breakthrough curve analysis and kinetics of fixed bed columns for Cu (II) cations using lignocellulosic wastes. BioResources. 10(1), 732-749.
- Delgado, J. & Águeda, V. & Uguina, M.& Sotelo, J. & Brea, P. & Grande, C. (2014). Adsorption and Diffusion of H2, CO, CH4, and CO2 in BPL Activated Carbon and 13X Zeolite: Evaluation of Performance in Pressure Swing Adsorption Hydrogen Purification by Simulation. Industrial & Engineering Chemistry Research (2014) 53 (40), 15414-15426.
- Espada García, David. Aprovechamiento energético de los gases de escape. Universidad Politécnica de Catalunya (UPC).
- Gobierno de España (2014). Ministerio de agricultura, alimentación y medio ambiente. Hoja de ruta de los sectores difusos a 2020.
- Gobierno de España (2020). Ministerio para la transición ecológica y el reto demográfico. Factores de emisión. Registro de huella de carbono, compensación y proyectos de absorción de dióxido de carbono (2018).
- Hauchhum, L., Mahanta, P (2014). Carbon dioxide adsorption on zeolites and activated carbon by pressure swing adsorption in a fixed bed. International Journal of Energy and Environmental Engineering 5, pages 349–356.
- Kouichi Kamiuto, Asami Goubaru & Ermalina (2006). Diffusion coefficients of carbon dioxide within type 13X zeolite particles. Chemical Engineering Communications, 193:5, pages 628-638.
- Luis, Patricia (2016). Use of monoethanolamine (MEA) for CO_2 capture in a global scenario: Consequences and alternatives. Desalination, Volume 380, pages 93-99.

- Mann M. (2019). Greenhouse Gases. Encyclopaedia Britannica [in line]. URL adress: <https://www.britannica.com/science/greenhouse-gas> [17/02/20]
- Matz M. & Knaebel K. (1990). Criteria for Selection of an Adsorbent for a Temperature Swing Process: Applied to Purification of an Aliphatic Solvent Contaminated with Aromatic Solutes. Separation Science and Technology, 25:9-10, pages 961-984.
- Sassykova L. R, Aubakirov Y. A, Sendilvelan S, Tashmukhambetova Z. K, Faizullaeva M. F, Bhaskar K, Batyrbayeva A. A, Ryskaliyeva R. G, Tyussyupova B. B, Zhakupova A. A. Sarybayev M. A. The Main Components of Vehicle Exhaust Gases and Their Effective Catalytic Neutralization (2019). Oriental Journal of Chemistry 2019;35(1).
- United Nations (UN) Environment Emissions Gap Reports (2018). The Intergovernmental Panel on Climate Change (IPCC).
- United States Environmental Protection Agency (EPA). Global greenhouse gases emissions data. URL adress:<https://www.epa.gov/ghgemissions/global-greenhouse-gas-emissions-data> [03/03/20]

NOMENCLATURE

Bi,o: Langmuir isotherm constant [cm^3/mg]

ΔU: Heat of adsorption [J/mol]

R: Ideal gas constant [J/K·mol]

bL: Langmuir isotherm parameter [cm^3/mg]

A: dimensionless parameter, $A = \frac{v_s R^2}{\varepsilon_L D_o Zz}$[-]

B: dimensionless parameter, $B = \frac{3(1-\varepsilon_L) k_f R}{\varepsilon_L D_o}$[-]

ηsat: dimensionless parameter, $\eta sat = \frac{qsat}{q_{ref}}$

C: Adsorbate gas phase concentration [mg/cm^3]

$C_{ref} = C_{in}$: Adsorbate initial concentration in gas phase [mg/cm^3]

Cs: Equilibrium concentration in the solid-gas interface [mg/cm^3]

dp: Particle diameter [cm]

dc: Column diameter [cm]

Do: Surface diffusion coefficient at q=0 [cm^2/s]

Ds: Surface diffusion coefficient [cm^2/s]

k: Dimensionless parameter in eq.1 [-]

kf: External mass transfer coefficient [cm/s]

Bi: dimensionless parameter, $Bi = \frac{k_f R C_{ref}}{\rho_s D_o q_{ref}}$

L: Bed length [cm]

q: Adsorbate mass fraction in solid phase [mg/g]

qref: Adsorbate mass fraction in equilibrium with Cref [mg/g]

qsat: Adsorbate saturation mass fraction in solid phase [mg/g]

Q: Flowrate [cm^3/s]

r: Radial position inside the adsorbent particle [cm]

R: Adsorbent particle radius [cm]

x: Dimensionless position in the adsorbent particle radius [-]

t: time [s]

τ: Dimensionless time [-]

vs: Superficial liquid velocity in bed [cm/s]

Zz: Axial position in bed [cm]

Z: Dimensionless axial position in bed [-]

T: Temperature of the adsorption process [K]

εL: Bed void fraction [-]

(1- εL): Bed fraction [-]

ρs: Apparent particle density [g/cm^3]

ρi: Density of component i at 1 bar and temperature of the experiment [g/cm^3]

ρgas: Density of the gas mixture at 1 bar and temperature of the experiment [g/cm^3]

μi: Dynamic viscosity of component i at 1 bar and temperature of the experiment [g/cm·s]

μgas: Dynamic viscosity of the gas mixture at 1 bar and temperature of the experiment [g/cm·s]

Δt: Dimensionless time step (variation of time per node)

n: Number of iterations

APPENDICES

APPENDIX 1: BREAKING TIME VS PARTICLE AND COLUMN DIAMETER

Particle diameter 0.03 cm and column diameter 15 cm

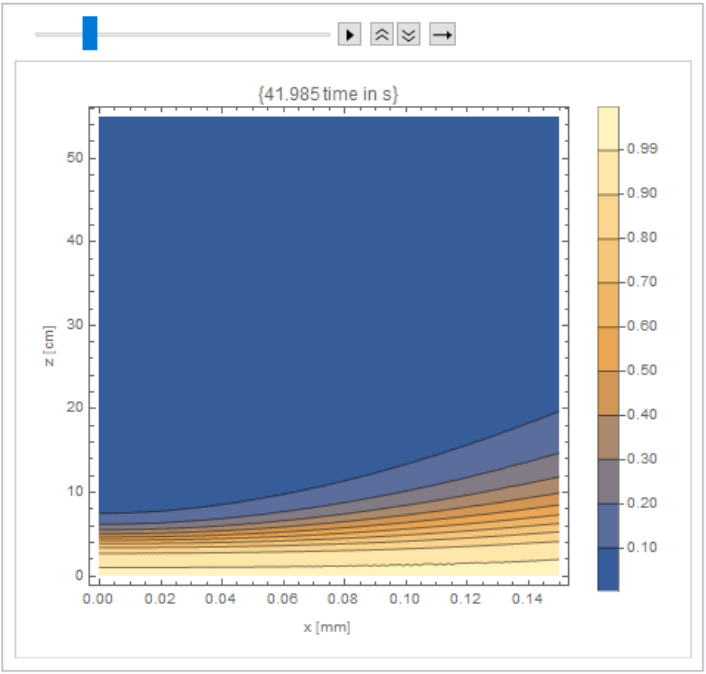

Figure 25. Dimensionless CO_2 concentration on solid phase at t = 42 s.

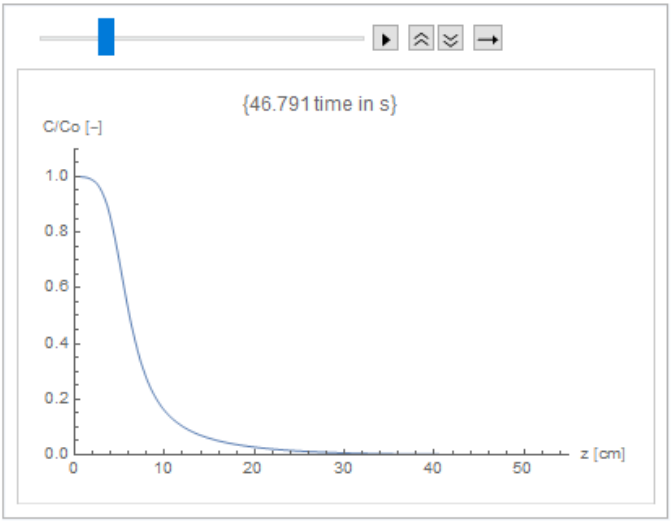

Figure 26. Dimensionless CO_2 concentration on gas phase at t = 47 s.

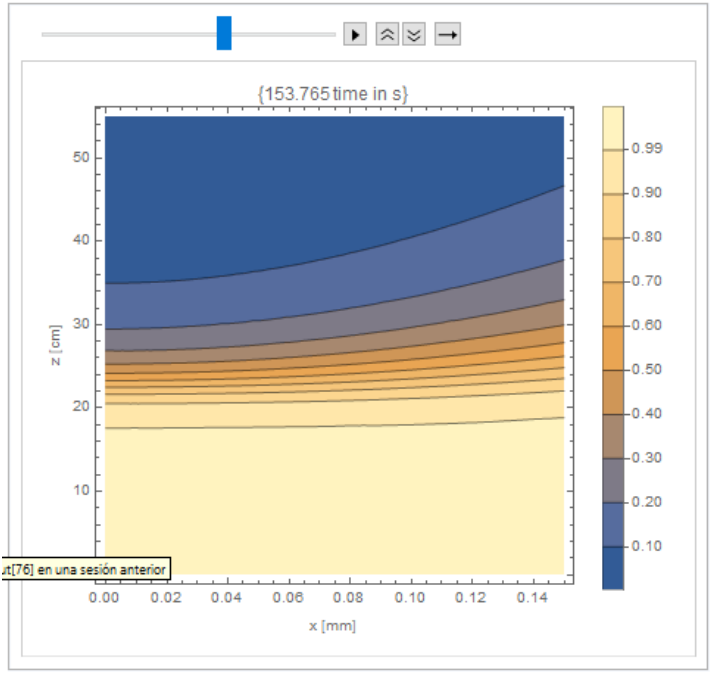

Figure 27. Dimensionless CO_2 concentration on solid phase at t = 154 s.

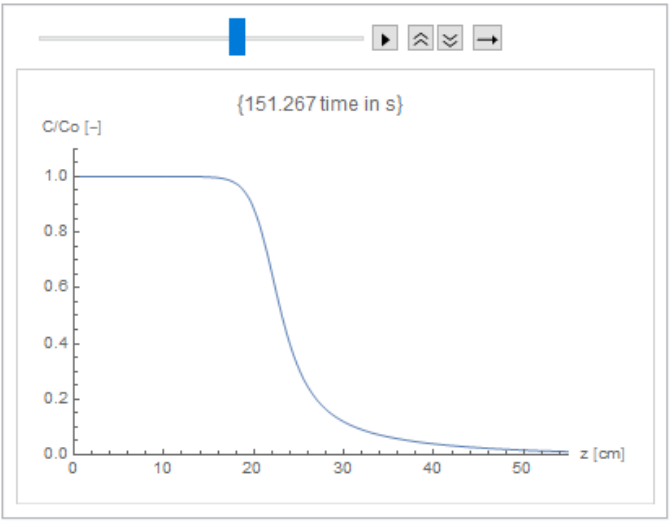

Figure 28. Dimensionless CO_2 concentration on gas phase at t = 151 s.

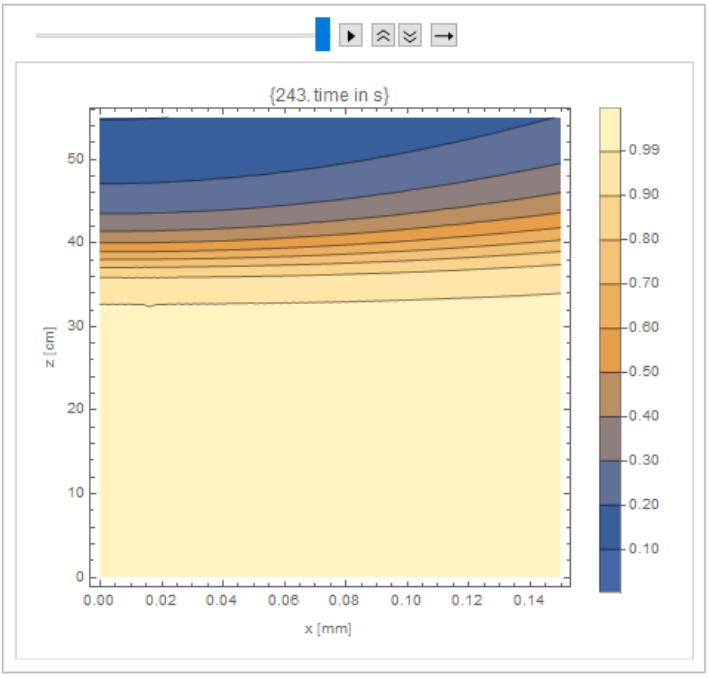

Figure 29. Dimensionless CO_2 concentration on solid phase at braking point, t = 243 s.

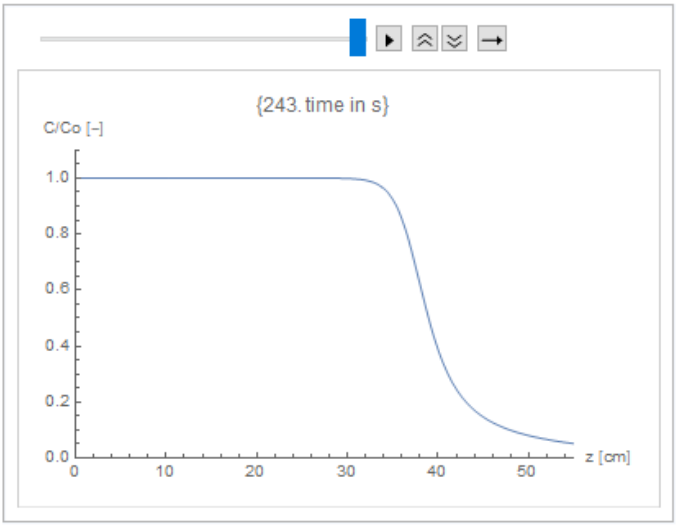

Figure 30. Dimensionless CO_2 concentration on gas phase at t = 243 s.

Particle diameter 0.03 cm and column diameter 20 cm

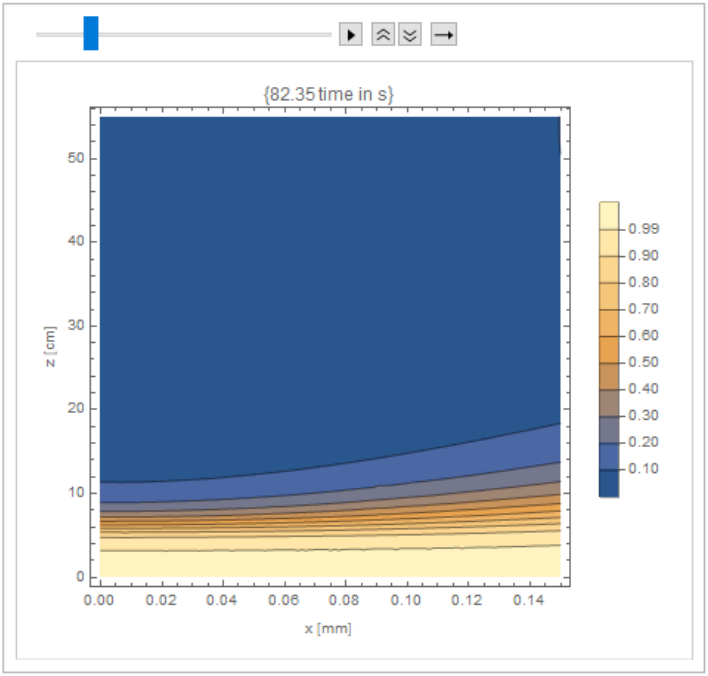

Figure 31. Dimensionless CO_2 concentration on solid phase at t = 82 s.

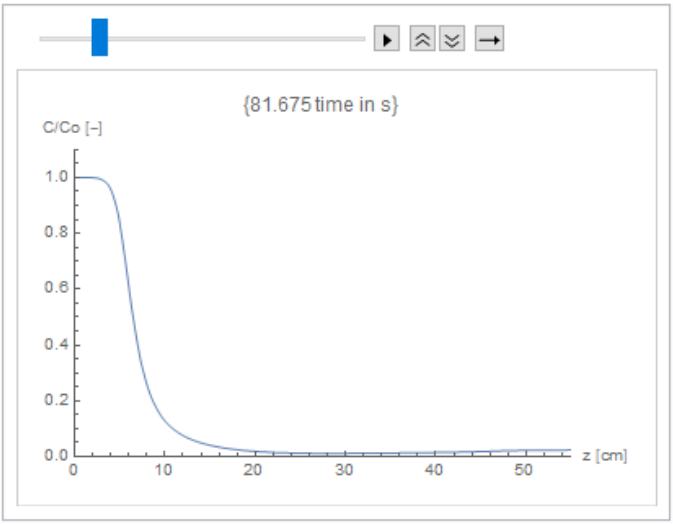

Figure 32. Dimensionless CO_2 concentration on gas phase at t = 82 s.

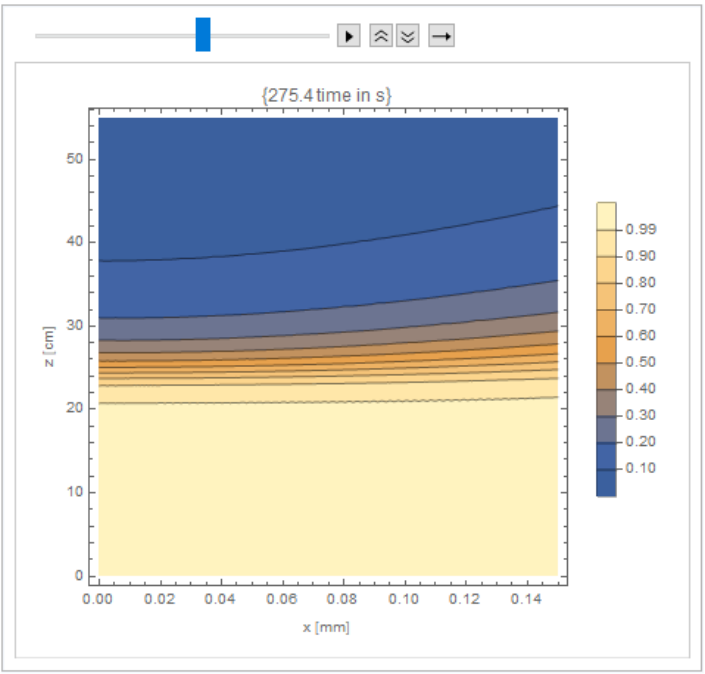

Figure 33. Dimensionless CO_2 concentration on solid phase at t = 275 s.

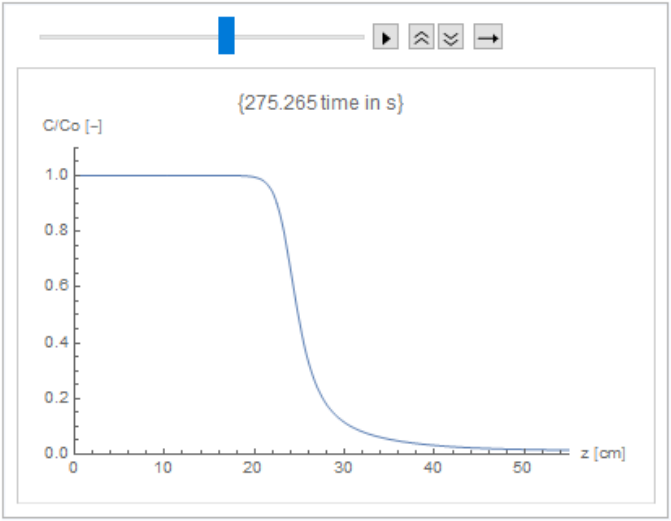

Figure 34. Dimensionless CO_2 concentration on gas phase at t = 275 s.

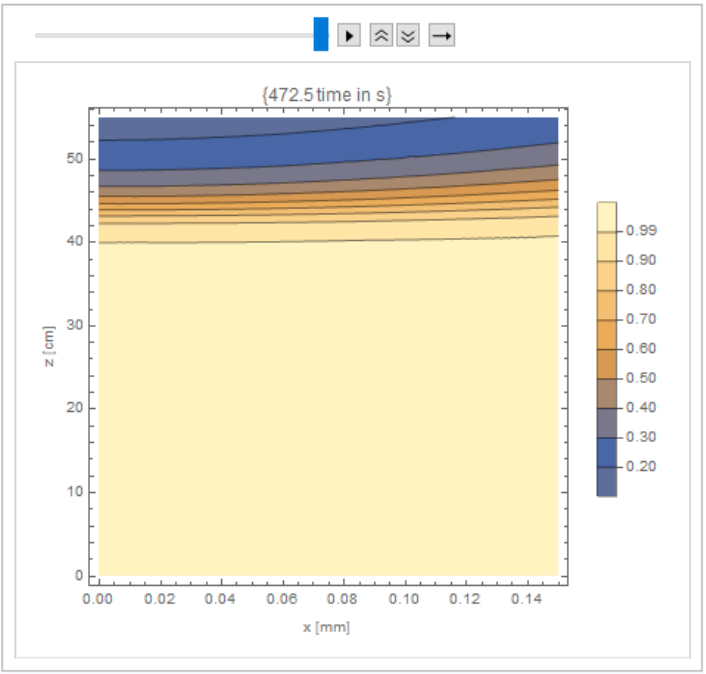

Figure 35. Dimensionless CO_2 concentration on solid phase at braking point, t =473 s.

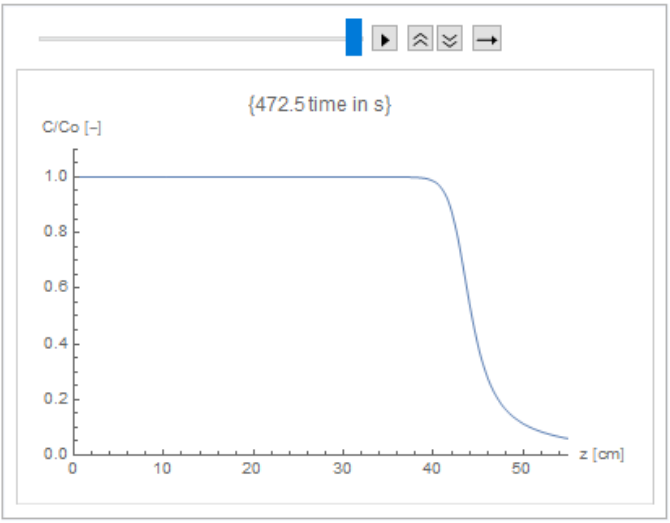

Figure 36. Dimensionless CO_2 concentration on gas phase at t = 473 s.

Particle diameter 0.03 cm and column diameter 25 cm

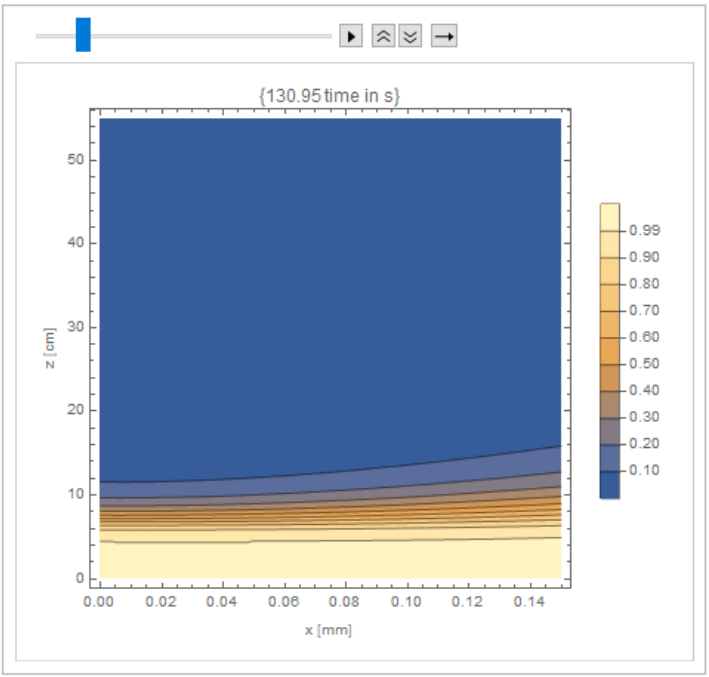

Figure 37. Dimensionless CO_2 concentration on solid phase at t = 131 s.

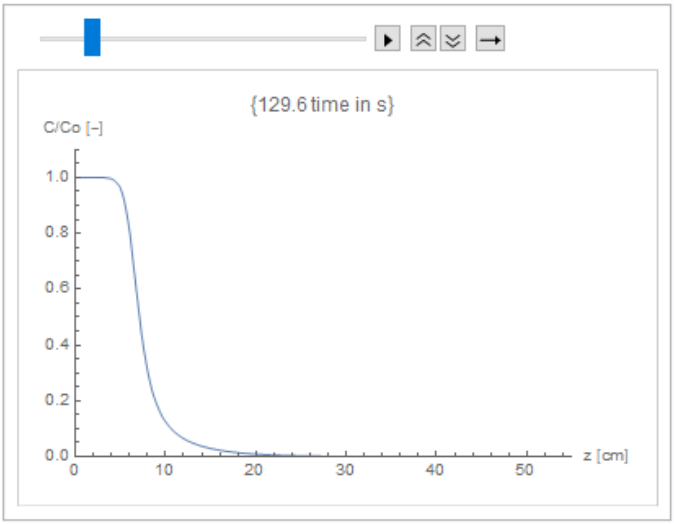

Figure 38. Dimensionless CO_2 concentration on gas phase at t = 130 s.

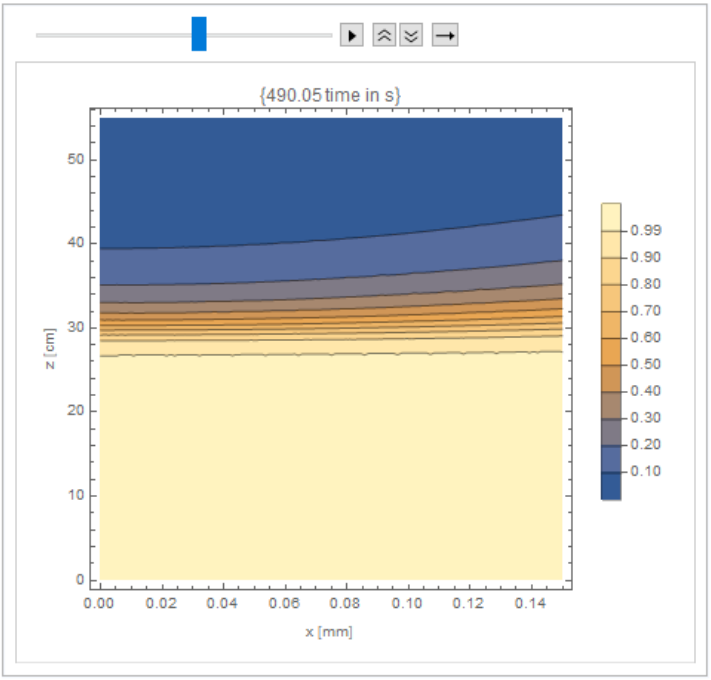

Figure 39. Dimensionless CO_2 concentration on solid phase at t = 490 s.

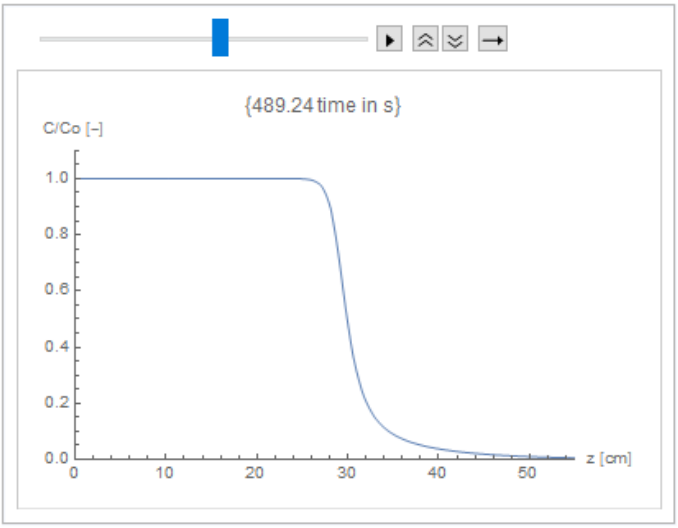

Figure 40. Dimensionless CO_2 concentration on gas phase at t = 489 s.

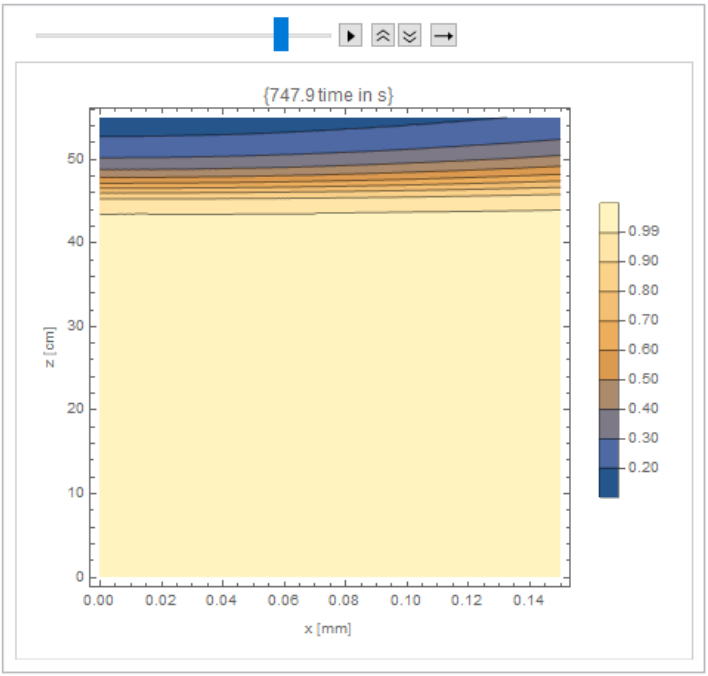

Figure 41. Dimensionless CO_2 concentration on solid phase at breaking point, t = 748 s.

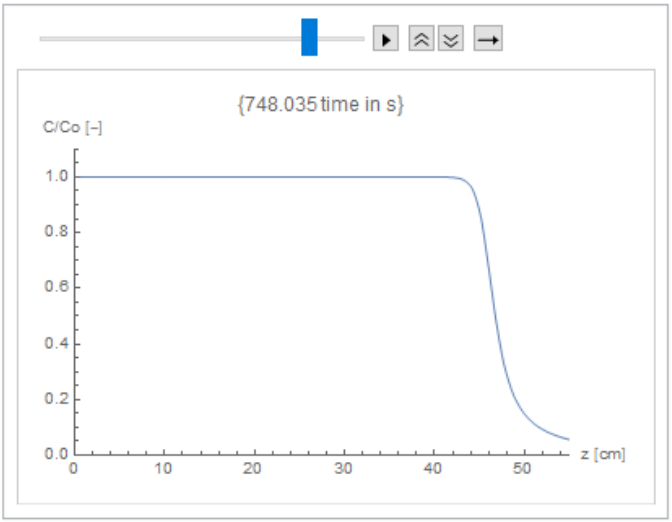

Figure 42. Dimensionless CO_2 concentration on gas phase at breaking point, t = 748 s.

Particle diameter 0.05 cm and column diameter 15 cm

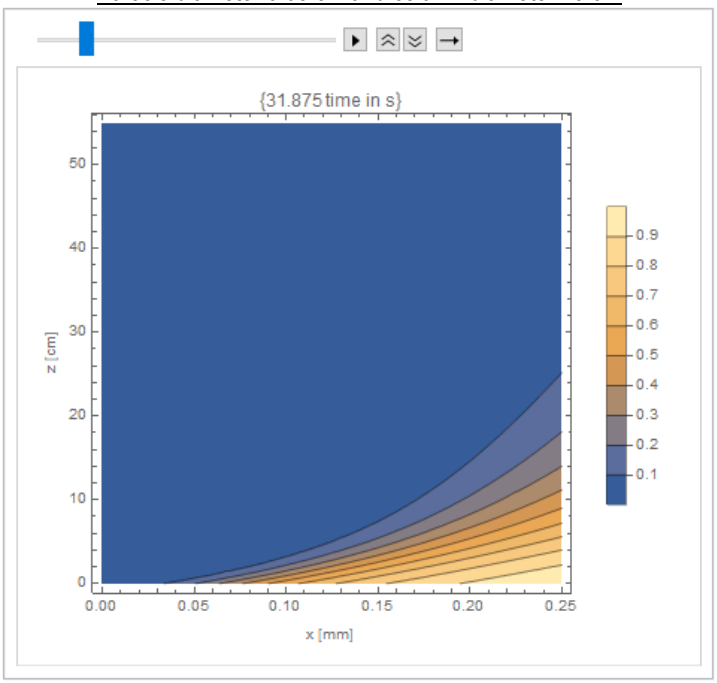

Figure 43. Dimensionless CO_2 concentration on solid phase at t = 32 s.

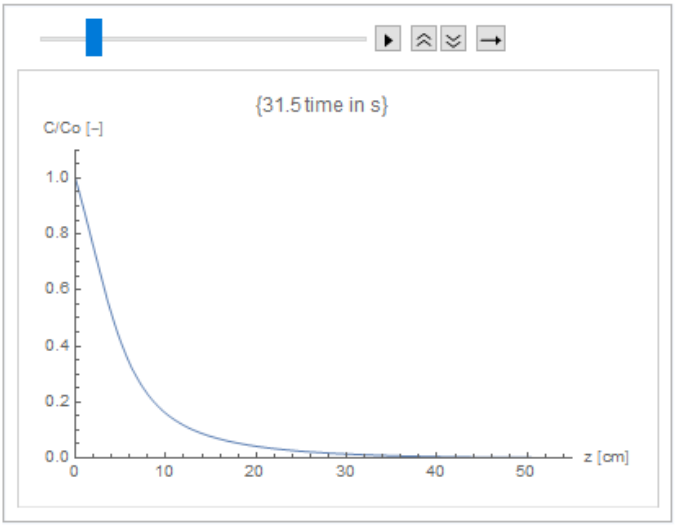

Figure 44. Dimensionless CO_2 concentration on gas phase at t = 32 s.

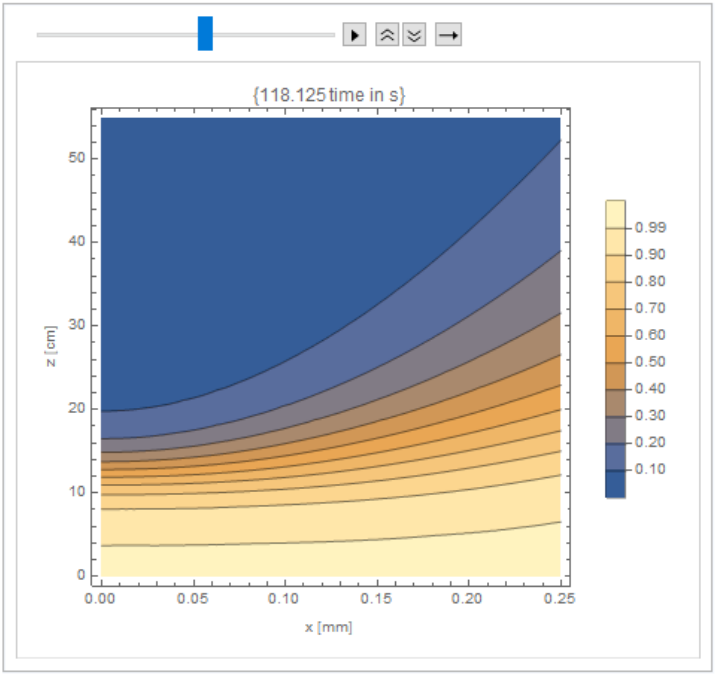

Figure 45. Dimensionless CO_2 concentration on solid phase at t=118 s.

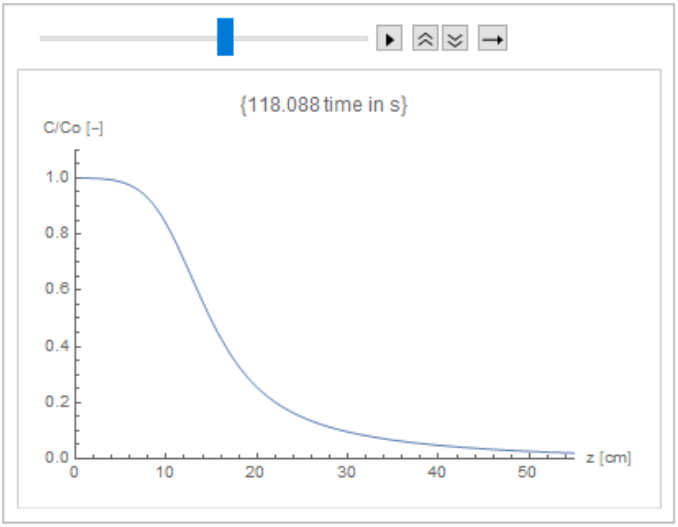

Figure 46. Dimensionless CO_2 concentration on gas phase at, t =118 s.

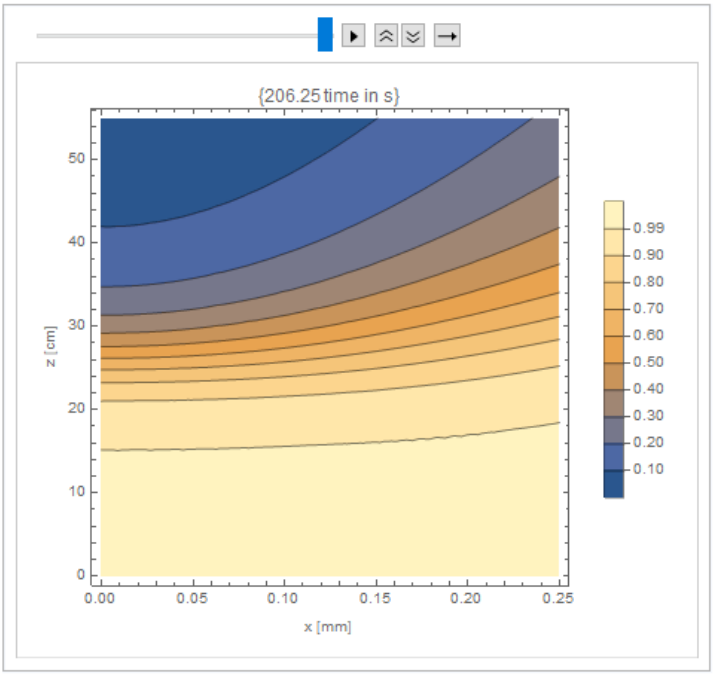

Figure 47. Dimensionless CO_2 concentration on solid phase at breaking point,t=206 s.

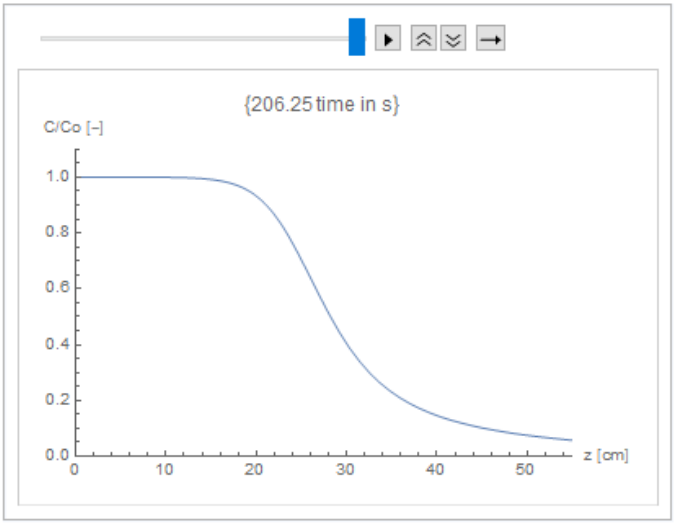

Figure 48. Dimensionless CO_2 concentration on gas phase at breaking point, t = 206 s.

Particle diameter 0.05 cm and column diameter 20 cm

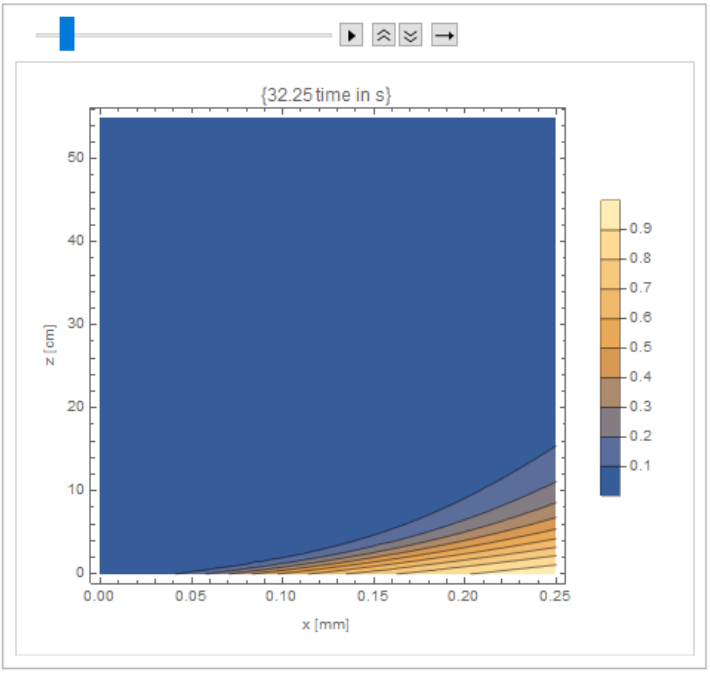

Figure 49. Dimensionless CO_2 concentration on solid phase at t = 32 s.

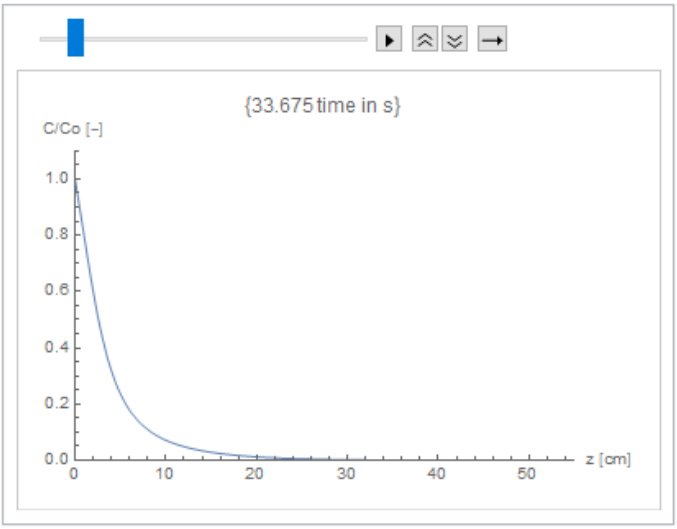

Figure 50. Dimensionless CO_2 concentration on gas phase at t = 34 s.

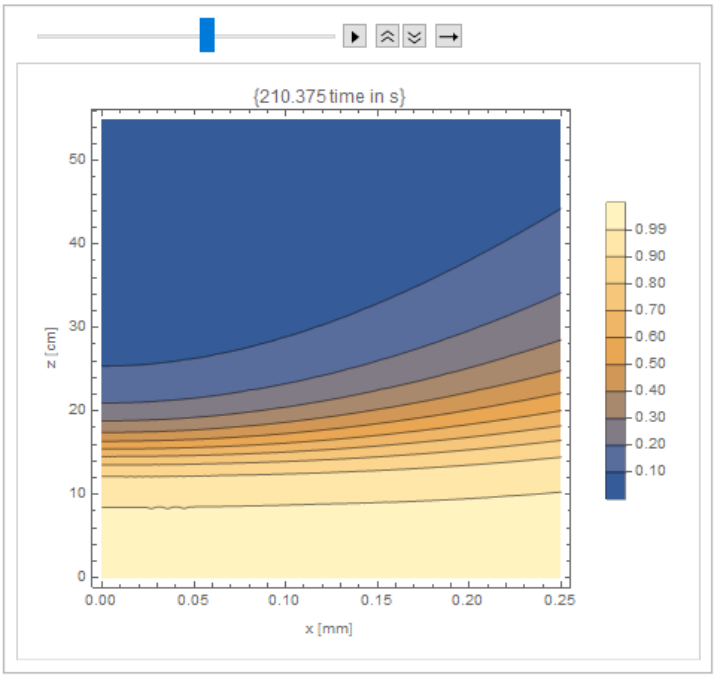

Figure 51. Dimensionless CO_2 concentration on solid phase at t = 210 s.

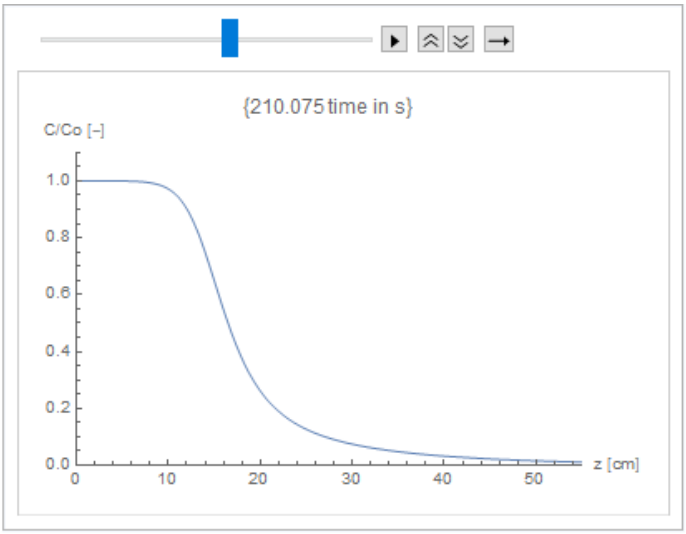

Figure 52. Dimensionless CO_2 concentration on solid phase at t = 210 s.

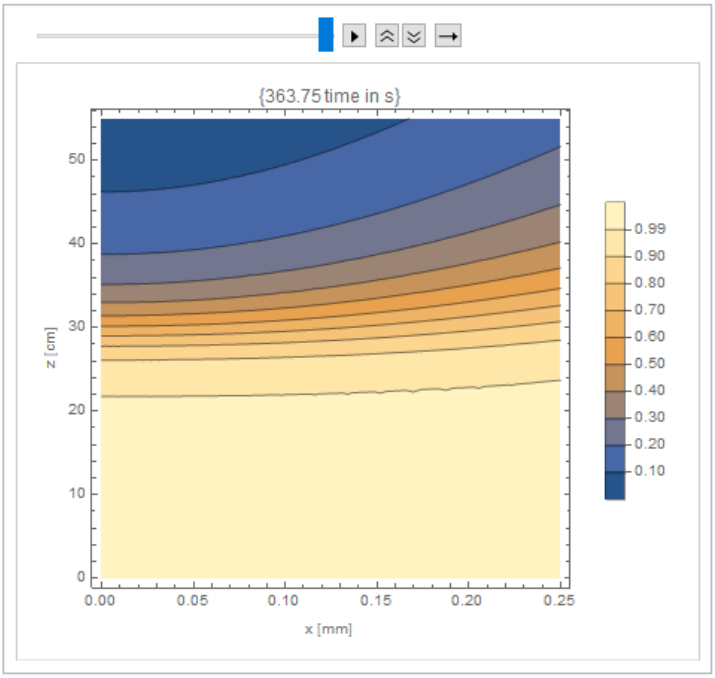

Figure 53. Dimensionless CO_2 concentration on solid phase at breaking point, t = 364 s.

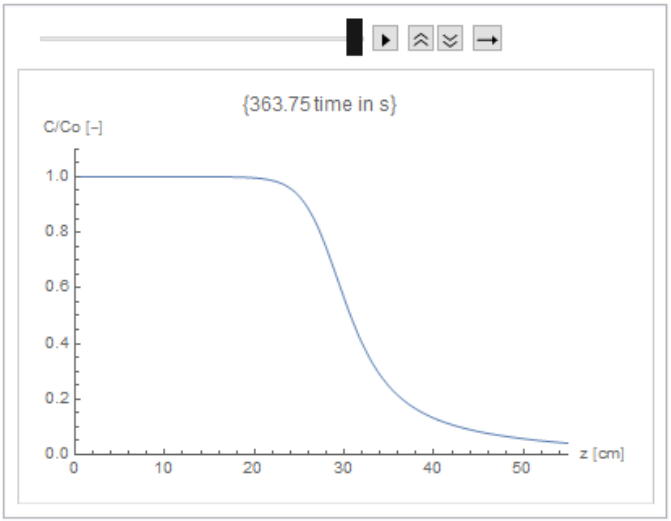

Figure 54. Dimensionless CO_2 concentration on gas phase at breaking point, t = 364 s.

Particle diameter 0.05 cm and column diameter 25 cm

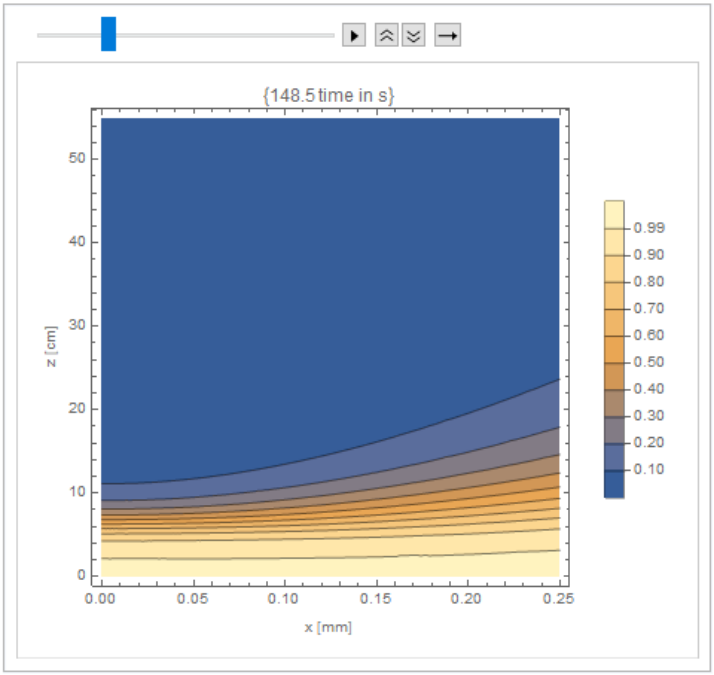

Figure 55. Dimensionless CO_2 concentration on solid phase at t = 149 s.

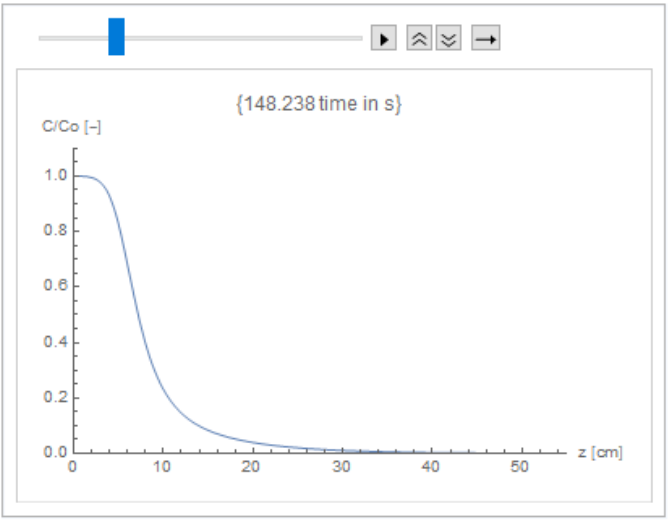

Figure 56. Dimensionless CO_2 concentration on gas phase at t = 148 s.

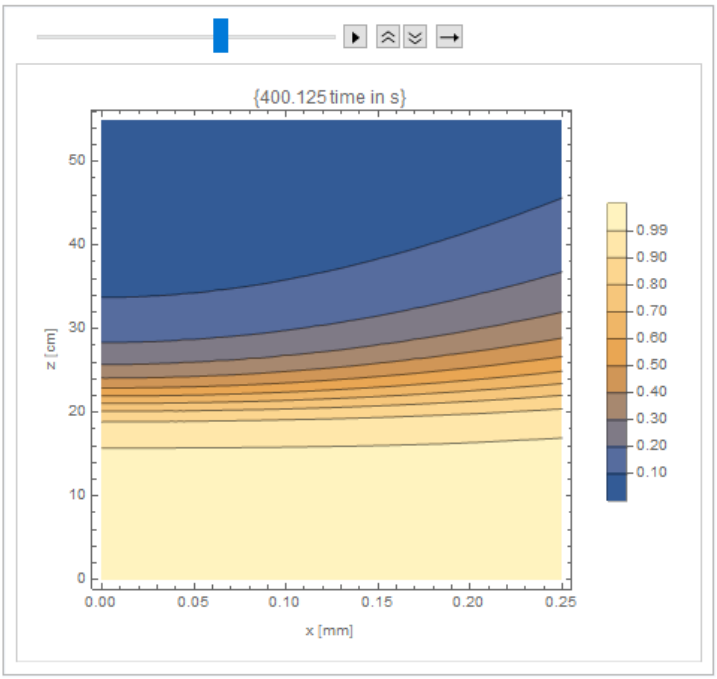

Figure 57. Dimensionless CO_2 concentration on solid phase at t = 400 s.

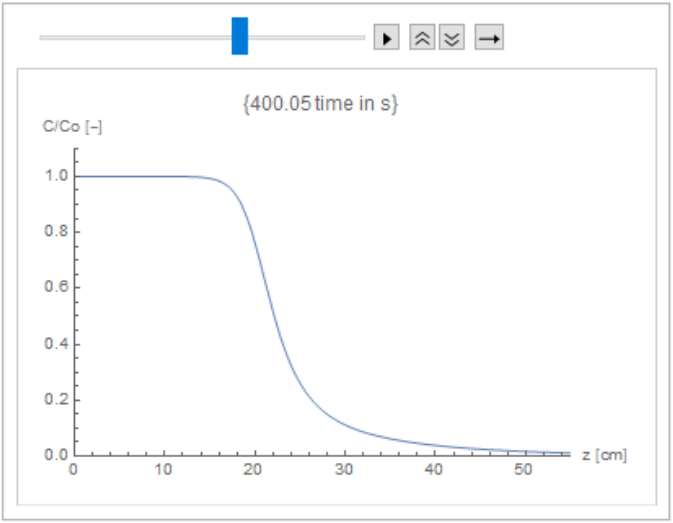

Figure 58. Dimensionless CO_2 concentration on gas phase at t = 400 s.

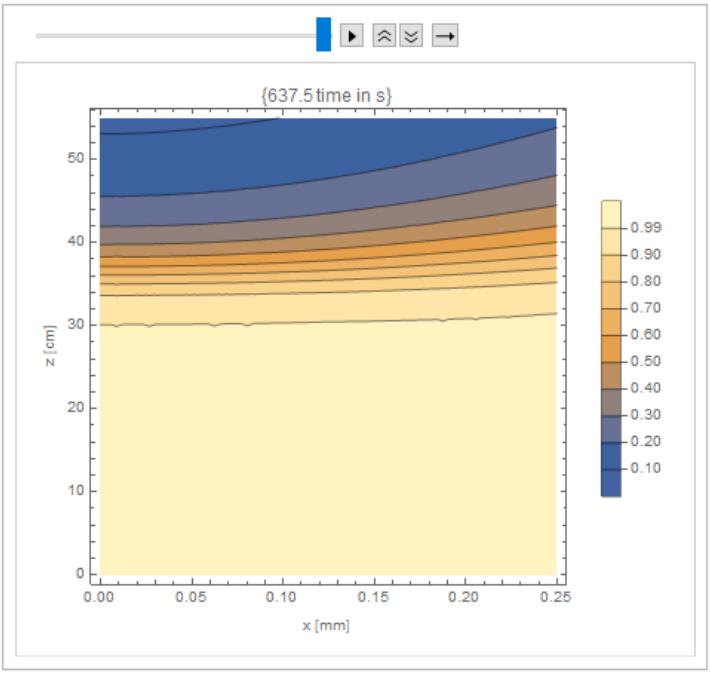

Figure 59. Dimensionless CO_2 concentration on solid phase at breaking point, t = 638 s.

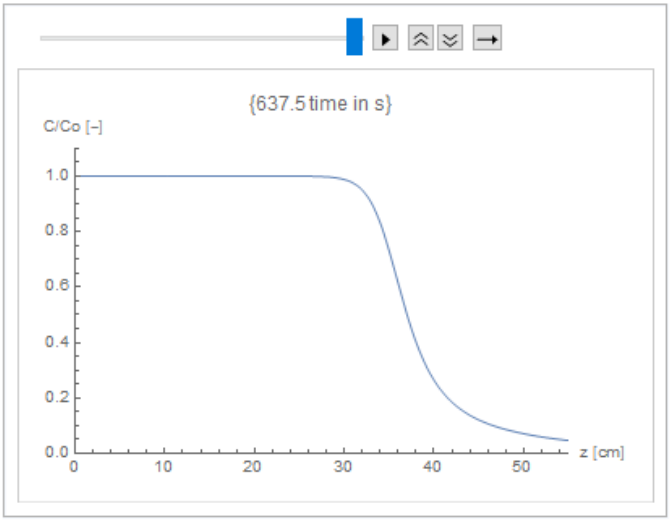

Figure 60. Dimensionless CO_2 concentration on gas phase at breaking point, t = 638 s.

Particle diameter 0.201 cm and column diameter 15 cm

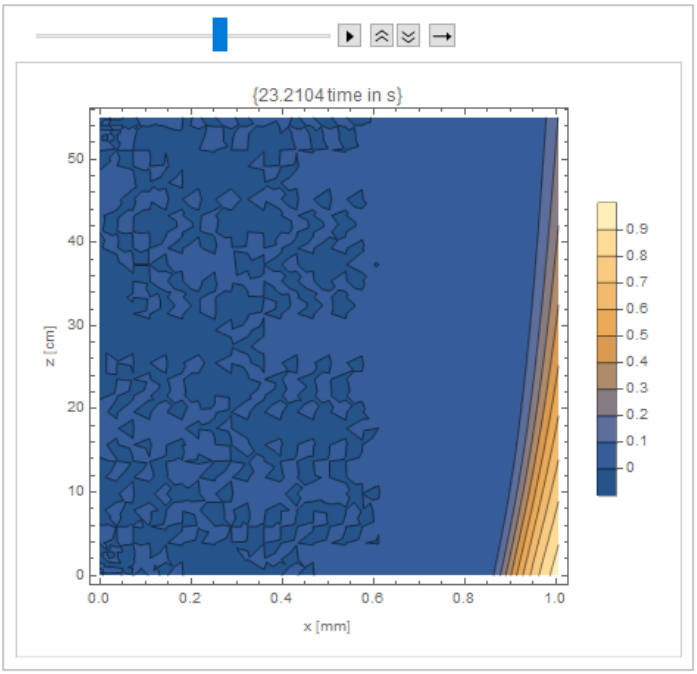

Figure 61. Dimensionless CO_2 concentration on solid phase at breaking point, t = 23 s.

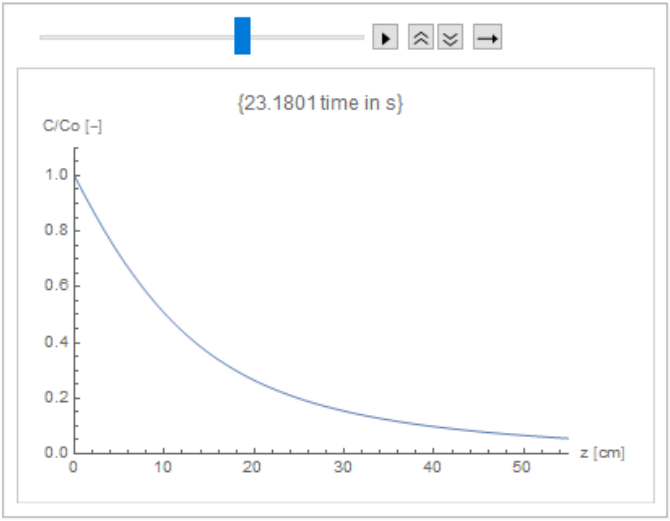

Figure 62. Dimensionless CO_2 concentration on gas phase at breaking point, t = 23 s.

Particle diameter 0.201 cm and column diameter 20 cm

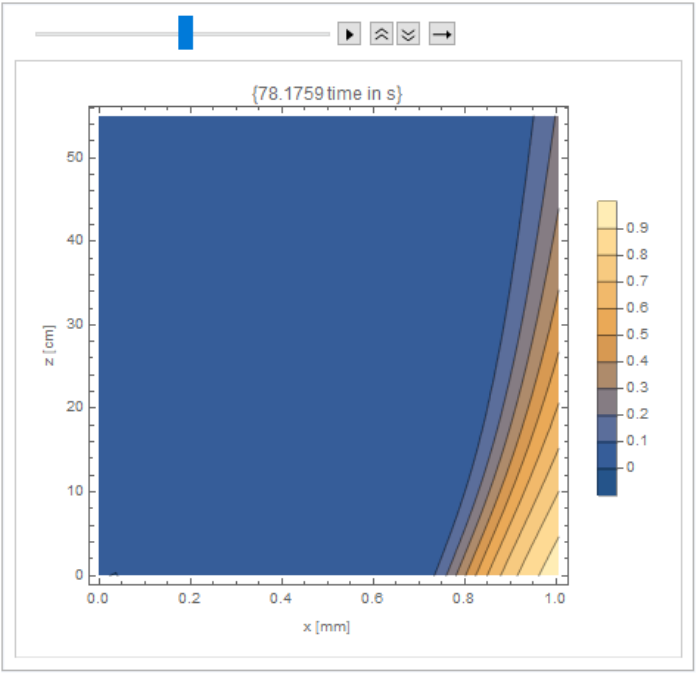

Figure 63. Dimensionless CO_2 concentration on solid phase at breaking point, t = 78 s.

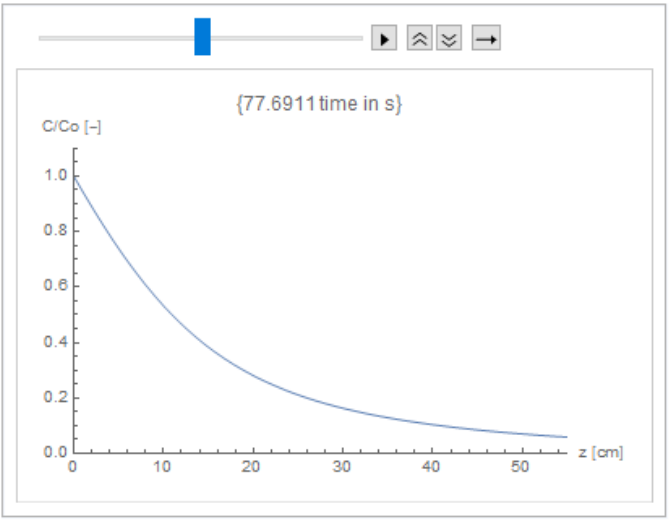

Figure 64. Dimensionless CO_2 concentration on gas phase at breaking point, t = 78 s.

Particle diameter 0.201 cm and column diameter 25 cm

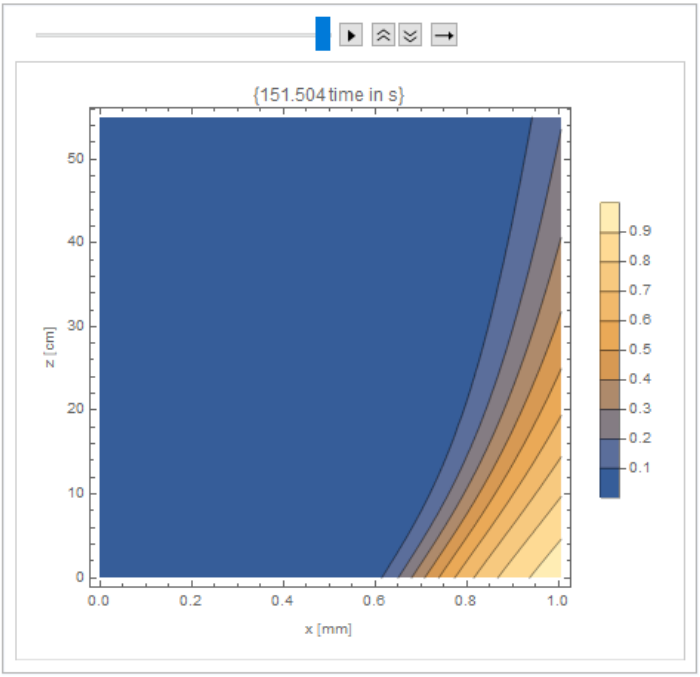

Figure 65. Dimensionless CO_2 concentration on solid phase at breaking point, t = 152 s.

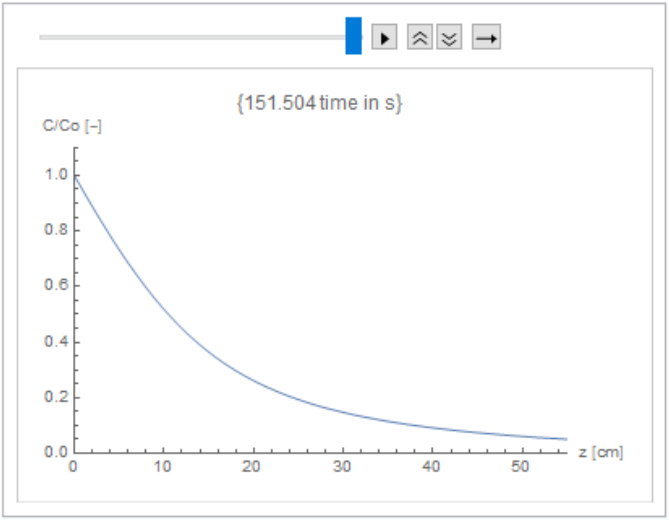

Figure 66. Dimensionless CO_2 concentration on gas phase at breaking point, t = 152 s.

Table 10. Breaking time depending on column and particle diameter.

		Particle diameter (cm)		
		0,03	0,05	0,201
Column diameter(cm)	Area (cm^2)	Breaking time (s)	Breaking time (s)	Breaking time (s)
0	0,00	0	0	0
15	176,71	243	206,25	23,18
20	314,16	472,5	363,8	77,7
25	490,87	748	637,5	151,5

APPENDIX 2: DISCRETIZED CODE

Time and space discretization

```
Time = 15 * 3600;
nz = 28; nr = 58; nt = 128;
Δt = N[Time / nt]; Δτ = Rationalize[Ds Time / R^2 nt]; Print["Δt =", N[Δt], " s,", "Δτ =", N[Δτ], "[-]"]

NN = nz + 1; ΔZZ = Lo / nz; Δξ = Rationalize[1 / nz]; Print["Δz =", N[ΔZZ], "cm,", "Δξ =", N[Δξ], "[-]"]
MM = nr + 1; ΔRr = N[R / nr]; Δρ = Rationalize[1 / nr]; Print["Δr =", ΔRr, " cm", "Δρ =", N[Δρ], "[-]"]
Print["Tiempo de registro =", Time / 3600, "h"]
```

Initial and boundary conditions

```
initialCond1 = Table[u_NN[0] = 0, {i, 1, NN}];
initialCond2 = Flatten[Join[Table[η_{i,j}[0] = 0, {i, 1, NN}, {j, 1, MM}]]];
boundaryCond1 = Flatten[Join[Table[u_1[τ] = 0, {τ, Δτ, nt Δτ, Δτ}]]];
```

Discretization of the equations

$$eq[i\_] := \left(1 + \Delta\tau\, B + A\,\frac{\Delta\tau}{\Delta\xi}\right) u_i[\tau] == A\,\frac{\Delta\tau}{\Delta\xi}\, u_{i-1}[\tau] + u_i[\tau - \Delta\tau] + \Delta\tau\, B\, \eta_{i,MM}[\tau];$$

$$eq[NN] := u_{NN}[\tau] == u_{NN-1}[\tau];$$

$$eqp[i\_, j\_] := \left(\Delta\rho + \frac{\Delta\tau}{\Delta\rho}\, E\text{^}\left(k\left(\frac{ra\,\eta_{i,j}[\tau - \Delta\tau]}{1 + ra\,\eta_{i,j}[\tau - \Delta\tau]}\right)\right) + \frac{\Delta\tau}{\Delta\rho}\, E\text{^}\left(k\left(\frac{ra\,\eta_{i,j}[\tau - \Delta\tau]}{1 + ra\,\eta_{i,j}[\tau - \Delta\tau]}\right)\right)\right)\eta_{i,j}[\tau] ==$$
$$\frac{\Delta\tau}{\Delta\rho}\, E\text{^}\left(k\left(\frac{ra\,\eta_{i,j}[\tau - \Delta\tau]}{1 + ra\,\eta_{i,j}[\tau - \Delta\tau]}\right)\right)\eta_{i,j-1}[\tau] + \frac{\Delta\tau}{\Delta\rho}\, E\text{^}\left(k\left(\frac{ra\,\eta_{i,j}[\tau - \Delta\tau]}{1 + ra\,\eta_{i,j}[\tau - \Delta\tau]}\right)\right)\eta_{i,j+1}[\tau] + \Delta\rho\,\eta_{i,j}[\tau - \Delta\tau];$$

$$eqp[i\_, 2] := \frac{\Delta\tau}{\Delta\rho}\, E\text{^}\left(k\left(\frac{ra\,\eta_{i,2}[\tau - \Delta\tau]}{1 + ra\,\eta_{i,2}[\tau - \Delta\tau]}\right)\right)\eta_{i,2}[\tau] ==$$
$$\frac{\Delta\tau}{\Delta\rho}\, E\text{^}\left(k\left(\frac{ra\,\eta_{i,2}[\tau - \Delta\tau]}{1 + ra\,\eta_{i,2}[\tau - \Delta\tau]}\right)\right)\eta_{i,3}[\tau] + \Delta\rho\,\eta_{i,2}[\tau - \Delta\tau];$$

$$eqp[i\_, 1] := \eta_{i,1}[\tau] == \eta_{i,2}[\tau];$$

$$eqp[i\_, MM] := -Bi\,\Delta\tau\, u_i[\tau - \Delta\tau] + Bi\,\Delta\tau\,\eta_{i,MM}[\tau] ==$$
$$-\frac{\Delta\tau}{\Delta\rho}\, E\text{^}\left(k\left(\frac{ra\,\eta_{i,MM-1}[\tau - \Delta\tau]}{1 + ra\,\eta_{i,MM-1}[\tau - \Delta\tau]}\right)\right)\frac{\frac{ra}{\rho}\,\eta_{i,MM}[\tau]}{1 + \frac{ra}{\rho}\,\eta_{i,MM}[\tau - \Delta\tau]} + \frac{\Delta\tau}{\Delta\rho}\, E\text{^}\left(k\left(\frac{ra\,\eta_{i,MM-1}[\tau - \Delta\tau]}{1 + ra\,\eta_{i,MM-1}[\tau - \Delta\tau]}\right)\right)\frac{\frac{ra}{\rho}\,\eta_{i,MM-1}[\tau]}{1 + \frac{ra}{\rho}\,\eta_{i,MM-1}[\tau - \Delta\tau]};$$

$$eqp[i\_, MM-1] := \left(\Delta\rho + \frac{1}{\frac{1}{Bi\,\Delta\tau\,\frac{p}{ra}\,(1+ra\,\eta_{i,MM}[\tau-\Delta\tau])} + \frac{1}{\frac{\Delta\tau}{\Delta\rho}E^{\wedge}\left(k\left(\frac{ra\,\eta_{i,MM-1}[\tau-\Delta\tau]}{1+ra\,\eta_{i,MM-1}[\tau-\Delta\tau]}\right)\right)}} + \frac{\Delta\tau}{\Delta\rho}E^{\wedge}\left(k\left(\frac{ra\,\eta_{i,MM-1}[\tau-\Delta\tau]}{1+ra\,\eta_{i,MM-1}[\tau-\Delta\tau]}\right)\right)\right)\eta_{i,MM-1}[\tau] ==$$

$$\frac{\Delta\tau}{\Delta\rho}E^{\wedge}\left(k\left(\frac{ra\,\eta_{i,MM-1}[\tau-\Delta\tau]}{1+ra\,\eta_{i,MM-1}[\tau-\Delta\tau]}\right)\right)\eta_{i,MM-2}[\tau] + \Delta\rho\;\eta_{i,MM-1}[\tau-\Delta\tau] +$$

$$+\left(\Delta\rho + \frac{1}{\frac{1}{Bi\,\Delta\tau\,\frac{p}{ra}\,(1+ra\,\eta_{i,MM}[\tau-\Delta\tau])} + \frac{1}{\frac{\Delta\tau}{\Delta\rho}E^{\wedge}\left(k\left(\frac{ra\,\eta_{i,MM-1}[\tau-\Delta\tau]}{1+ra\,\eta_{i,MM-1}[\tau-\Delta\tau]}\right)\right)}}\right)u_i[\tau-\Delta\tau];$$

Equation aggrupation depending on the mass balance

```
eqns = Flatten[Join[Table[eq[i], {i, 2, NN - 1}], {eq[NN]}]];
eqnsspp = Flatten[Join[Table[eqp[i, j], {i, 1, NN}, {j, 3, MM - 2}], Table[eqp[i, 1], {i, 1, NN}],
    Table[eqp[i, 2], {i, 1, NN}], Table[eqp[i, MM - 1], {i, 1, NN}], Table[eqp[i, MM], {i, 1, NN}]]];
```

Solving the equations for all the time and column length

```
n = 0;
Do[n = 1 + n; Rationalize[τ = n Δτ];
 unknown = Flatten[Join[Table[u_i[τ], {i, 2, NN}]]];
 m = 0; Do[m = 1 + m;
  eqnsp = Flatten[Join[Table[eqp[m, j], {j, 3, MM - 2}], {eqp[m, 1], eqp[m, 2], eqp[m, MM - 1], eqp[m, MM]}]];
  unknownp = Flatten[Join[Table[η_{m,j}[τ], {j, 1, MM}]]];
  solutionP = NSolve[eqnsp, unknownp][[1]];
  Table[η_{m,j}[τ] = η_{m,j}[τ] /. solutionP, {j, 1, MM}]; {NN}]; solution = NSolve[eqns, unknown][[1]];
 Table[u_i[τ] = u_i[τ] /. solution, {i, 2, NN}]; {nt}]
solution1 = Table[u_i[τ], {τ, 0, nt Δτ, Δτ}, {i, 2, NN}];
solution2 = Table[η_{i,j}[τ], {τ, 0, nt Δτ, Δτ}, {i, 1, NN}, {j, 1, MM}];
MatrixForm[solution1];
MatrixForm[solution2];
```